



**HAL**  
open science

## Numerical simulations of adhesive spreading during bonding-induced squeeze

Lorraine Aparecida Silva, Christine Espinosa, Eric Paroissien, Frédéric Lachaud, Lucas F.M. da Silva

► **To cite this version:**

Lorraine Aparecida Silva, Christine Espinosa, Eric Paroissien, Frédéric Lachaud, Lucas F.M. da Silva. Numerical simulations of adhesive spreading during bonding-induced squeeze. *The Journal of Adhesion*, 2021, pp.0. 10.1080/00218464.2021.1982388 . hal-03360104

**HAL Id: hal-03360104**

**<https://hal.science/hal-03360104v1>**

Submitted on 30 Sep 2021

**HAL** is a multi-disciplinary open access archive for the deposit and dissemination of scientific research documents, whether they are published or not. The documents may come from teaching and research institutions in France or abroad, or from public or private research centers.

L'archive ouverte pluridisciplinaire **HAL**, est destinée au dépôt et à la diffusion de documents scientifiques de niveau recherche, publiés ou non, émanant des établissements d'enseignement et de recherche français ou étrangers, des laboratoires publics ou privés.



## Open Archive Toulouse Archive Ouverte (OATAO)

OATAO is an open access repository that collects the work of some Toulouse researchers and makes it freely available over the web where possible.

This is an author's version published in: <https://oatao.univ-toulouse.fr/28337>

**Official URL :** <https://doi.org/10.1080/00218464.2021.1982388>

### To cite this version :

Aparecida Silva, Lorraine and Espinosa, Christine and Paroissien, Eric and Lachaud, Frédéric and da Silva, Lucas F.M. Numerical simulations of adhesive spreading during bonding-induced squeeze. (2021) Numerical simulations of adhesive spreading during bonding-induced squeeze. ISSN 1545-5823

Any correspondence concerning this service should be sent to the repository administrator:

[tech-oatao@listes-diff.inp-toulouse.fr](mailto:tech-oatao@listes-diff.inp-toulouse.fr)

# Numerical simulations of adhesive spreading during bonding-induced squeeze

Lorraine Aparecida Silva <sup>a</sup>, Christine Espinosa<sup>a</sup>, Eric Paroissien<sup>a</sup>, Frédéric Lachaud<sup>a</sup>, and Lucas F.M. da Silva<sup>b</sup>

<sup>a</sup>Institut Clément Ader (Ica), Université De Toulouse, Isae-superaero, Insa, Imt Mines Albi, Utiii, Cnrs, 3 Rue Caroline Aigle, Toulouse, France; <sup>b</sup>Department of Mechanical Engineering, Faculty of Engineering, University of Porto, Porto Portugal

## ABSTRACT

The current work is intended to give an overview of issues related to the numerical simulation of adhesive spreading for liquid to semi-liquid adhesives. The advantages and limitations are presented in order to guide the choice of the suitable approach depending on the case under consideration. It is shown that methods are of two categories, whether they are grid-based or meshless. In the first, the movement of the matter is directly dependent on the mesh size and distribution. Contrariwise, in the meshfree methods, the particles are free to move and each carries its properties. Besides, cases of application are presented to provide a database for calculating adhesive spreading with the particulate SPH method. It is shown that it is possible to use simple behaviour laws to win this case.


## KEYWORDS

Spreading < methods of analysis; rheology < methods of analysis; numerical analysis < methods of analysis; bonding < applications; SPH < methods of analysis; fluid mechanics < methods of analysis

## 1. INTRODUCTION

The increasing use of structural bonding raises the question of the quality of the assembly for structural strength (strength requirement) and disassembly at end of life (structural life cycle analysis). In parallel, taking environmental protection into account, or even basing the design of new structures on it, is a growing concern in all fields of industries and in particular in aeronautics. As an example of direct constraint, the REACH procedure<sup>1</sup> standing for “Registration, Evaluation and Authorisation of Chemicals” is a European initiative to regulate the use of dangerous materials to enhance the protection of the environment while maintaining the competitiveness of the industry. In the field of aerospace engineering, the European Space Agency (ESA) promotes Design for Demise.<sup>2</sup> Indeed, when they reach the end of their service life, satellites are no longer controlled and powered. They are then expected to

---

**CONTACT** Lorraine Aparecida Silva  [lorraine.silva@isae-superaero.fr](mailto:lorraine.silva@isae-superaero.fr)  Institut Clément Ader (Ica), Université De Toulouse, Isae-superaero, Insa, Imt Mines Albi, Utiii, Cnrs, 3 Rue Caroline Aigle, Toulouse 31400, France

<sup>1</sup><https://echa.europa.eu/fr/regulations/reach/understanding-reach>

<sup>2</sup>[https://www.esa.int/Enabling\\_Support/Preparing\\_for\\_the\\_Future/Discovery\\_and\\_Preparation/Design\\_for\\_demise\\_bringing\\_spacecraft\\_down\\_safely\\_and\\_efficiently](https://www.esa.int/Enabling_Support/Preparing_for_the_Future/Discovery_and_Preparation/Design_for_demise_bringing_spacecraft_down_safely_and_efficiently)

begin their slow descent into the Earth atmosphere and either completely burn up or are controlled to come down into the oceans. It is up to the company to ensure that the satellite is completely burned up and disintegrated during re-entry if this option is selected.<sup>3</sup> But some accidents have occurred, such as fuel tank re-entry<sup>4</sup> or debris falling on people.<sup>5</sup> This situation is no longer acceptable, so designing satellites for controlled disassembly is the approach recommended by ESA. Furthermore, growing concerns about environmental issues have led industries to focus on technologies for mass reduction and meeting requirements for durability, performance, and production costs for structures. In these circumstances, adhesive joints have begun to gain in visibility and investments.

Structural bonding is an extensively used technique for joining substrates of different mechanical characteristics. In short, an adhesive joint consists of two or more adherents held together by adhesion and it allows the transfer of mechanical forces through the interface. Adhesive bonding is known to offer an elevated strength-to-mass ratio, which is a critical stake for the automotive and aeronautical industries, for example<sup>[1]</sup>. The strength of the structural bonding itself is likely to be affected by the quality of the adhesive mechanical properties playing a role of a solid layer between the substrates. These are the results of the adhesive slip/stick capability in its liquid or viscoplastic state during the bonding process<sup>[2]</sup>. In particular, bubbles and pores created during deposition on the substrates or during the approach of the substrates and squeezing of the adhesive between the substrates affect the strength of the system's assembly<sup>[3,4]</sup>. In addition to the mechanical characteristics, the adhesive joints provide electrical isolation for electrical components and increase damping properties, possibly due to their viscoelastic behaviour. Another concern in eco-design is the consideration of debonding on demand. As there may be a need to separate or recycle the primitive materials of substrates, the joint can be asked to have a dual role of strengthening the assembly structure during the product life and to separate it after life in a clean way. This separation is often described in the literature as using techniques that depend on the addition of components in the joint. For example, disassembly based on thermal debonding<sup>[5]</sup> depends on the expandable particles or on chemical mechanisms with additives that can change viscosity<sup>[6,7]</sup>. In all of these cases it is important to optimize the deposition and interaction between the adhesive and the substrates, besides the recovering area. Depending on the adherent configuration to be joined, adhesive spreading is performed under constraints and this process also generates remaining constraints. Furthermore, the adhesive joint can also suffer from premature ruptures due to imperfections in adhesive layer deposition, uncovered surfaces or non-

---

<sup>3</sup><http://www.astrosurf.com/luxorion/Images/mir-reentry-dwg.png>

<sup>4</sup><https://aerospace.org/space-debris>

<sup>5</sup><https://aerospace.org/article/satellite-reentry-manipulating-plunge>

uniform thickness. Figure 1 shows examples of adhesive joint configurations currently used in industrial applications. A bonding strategy is then necessary to improve the adhesive deposition, which is a factor of primary importance on durability.

It is then of primary concern to be able to control adhesive spreading during the bonding process. Model-based engineering and computational mechanics are commonly considered as the best and cheapest forms, if compared with experimental tests, to evaluate the different scenarios and can be useful in reducing the experimental tests necessities. This multi-physical problem is addressed by various numerical strategies in the literature, depending on the hypothesis adopted. This paper presents a general description of the physical phenomena involved in adhesive squeeze in section 2 ‘Phenomenology’ and also gives a synthesis of the numerical methods and models that can be applied to simulate and predict adhesive squeeze during the bonding in section 3 ‘Discretization and approximation’. The last section is dedicated to an application case using the Smooth Particle Method (SPH) and its comparison with experimental observations of adhesive squeeze between two plane plates.

## 2. PHENOMENOLOGY OF ADHESIVE SPREADING

Understanding adhesive behaviour and its rheology is the first step toward building a numerical model capable of representing the adhesive during the bonding process and this identification is, in general, made through experimental tests <sup>[1]</sup>. The manufacturing process of bonded joints is a multi-physical subject composed of several steps that drive the properties of the resulting joint. Assuming the nature of adherents is prescribed, the first step is

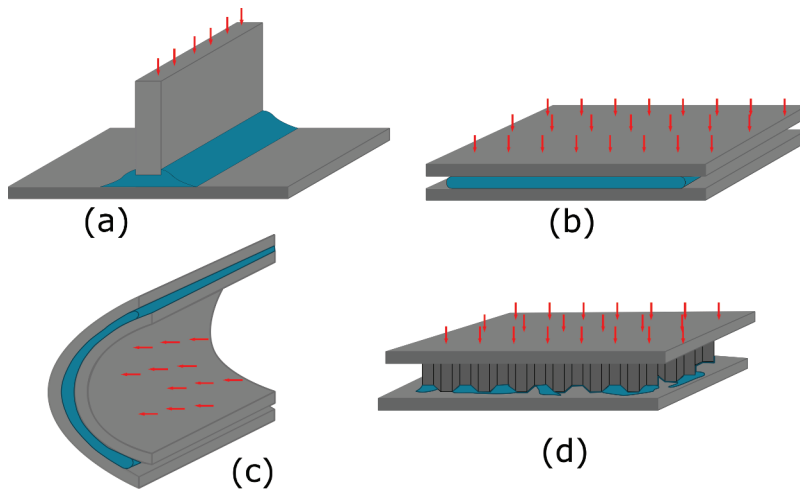


**Figure 1.** Squeeze flow with a constant mass in different configurations (a) Joint in T format, (b) Joint between plane plates, (c) Joint between curve plates, (d) Joint in a sandwich structure.

the choice of the adhesive, which includes the definition of the surface preparation, deposition, spreading and curing process. In adhesion theories, many factors influence the final behaviour of joints, among which wetting and spreading are the most important factors <sup>[1]</sup>.

## 2.1. Adhesive deposition, wettability and spreading

Deposition of the adhesive on the substrates is the first step of the bonding process. The deposition depends on the wetting capability of the adhesive itself, and on the wettability of the substrates, leading to the question of fluid-structure interaction <sup>[8]</sup>. Wetting is the ability of a liquid to enter into contact with a solid and results from intermolecular interactions. For an adhesive, wettability is mainly related to viscosity and density. For adherents, it is related to roughness.

The contact angle provides a measure of the interaction between the liquid and the surface. It is possible to establish that good wettability is achieved when Classification of fluids in rheology behaviours (see Figure 2a). On the other hand, the larger is the contact angle, e.g. close to  $180^\circ$ , the worse the wettability, as shown in Figure 2b. In the extreme case (Classification of fluids in rheology behaviours), the liquid becomes a thin film and this phenomenon is called spreading, as shown in Figure 2c <sup>[1]</sup>. If this angle is considered as a descriptive parameter of the interaction between the adhesive and the substrates, it is not a parameter that is used in numerical models or in behaviour laws to control the final spreading or the final thickness of the joint.

Spreading is the action of covering a surface and can occur naturally or in a forced way. The forced way implies the application of some force until the equilibrium state of forces and/or the fully covered. This process has direct influence on the final thickness of the adhesive layer in the joint. Furthermore, the joint's mechanical performances are highly dependent on the adhesive layer's properties and its thickness<sup>[9,10]</sup>. The role of the adhesive in several applications therefore began to change with joint functionalization. The objective is to use components that are already there for structural motives, giving them a second function. For example, the adhesive joint can be used as a resource to create weakness zones, if disassembly is necessary.

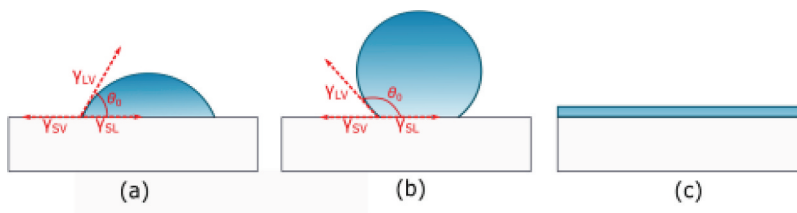


**Figure 2.** Schematic representation static contact angles (Classification of fluids in rheology behaviours); (a) "good" wet; (b) "poor" wet; (c) spreading.

Spreading squeeze is, in the simplest case, when a fluid is deformed between two parallel or nearly parallel boundaries approaching each other and pressing it. A description of the physical problem and the associated hypotheses can be consulted in <sup>[11,12]</sup>, where the authors show the influence of the chosen behaviour law to describe the fluid and the effect of boundary conditions on the adhesive distribution. Besides the configuration of two plane plates, adhesive squeeze along with other configurations represents a challenge, for example, for the squeeze between annular plates, where the conditions for correct adhesive distribution depends on geometrical parameters <sup>[13]</sup>, as well the adhesive properties and surface properties <sup>[14]</sup>. Another case is when one of the surfaces presents obstacles, which can improve adhesion in cases with low viscosity or, on the contrary, with a highly viscous adhesive <sup>[15]</sup>. Another very interesting case of the influence of adhesive squeeze concerns the assembly of sandwich structures. Distribution of the adhesive is an issue because air or gas trapped in the cells can flow through the adhesion line during curing, and some non-uniform distribution could occur between adjacent cells, both leading to poor quality of the bonding <sup>[16,17]</sup>. In conclusion, spreading depends on the adhesive behaviour, adherents' configuration composition and curing process. Its simulation is necessary to help design the bonding process, and thus to be able to reduce the risk of adhesive spillage and to control the joint's final properties.

## **2.2. Behaviour laws**

The rheology of solids and fluids are in many respects similar. Nevertheless, if both are displaced and deformed under applied forces, displaced fluid materials adapt their external boundary to the solid external frame or container, while solid materials offer a their own external shape. One exception is a viscous or gelatine fluid that can exhibit fluid or solid behaviour, depending on its viscosity. Viscosity of adhesives is driven by the polymerisation level and can exhibit both behaviours. Before the curing process, the adhesive is in a liquid state and is submitted to a flow during the bonding process. Once the curing process is finished, it becomes a solid.

The behaviour of a solid material is usually described by two relationships between fluxes of internal forces (stresses) and deformations (strains): the first is the deviatoric resistance to shear deformation; the second is the spherical pressure resistance to volume change. Pure fluids do not offer deviatoric resistance. As a consequence, at rest they suffer from creep deformation. Only pressure or mean compressive stress can resist the external forces or prescribed deformations <sup>[18]</sup>. The rheological properties depend on the material characteristics and mechanical load <sup>[19]</sup>.

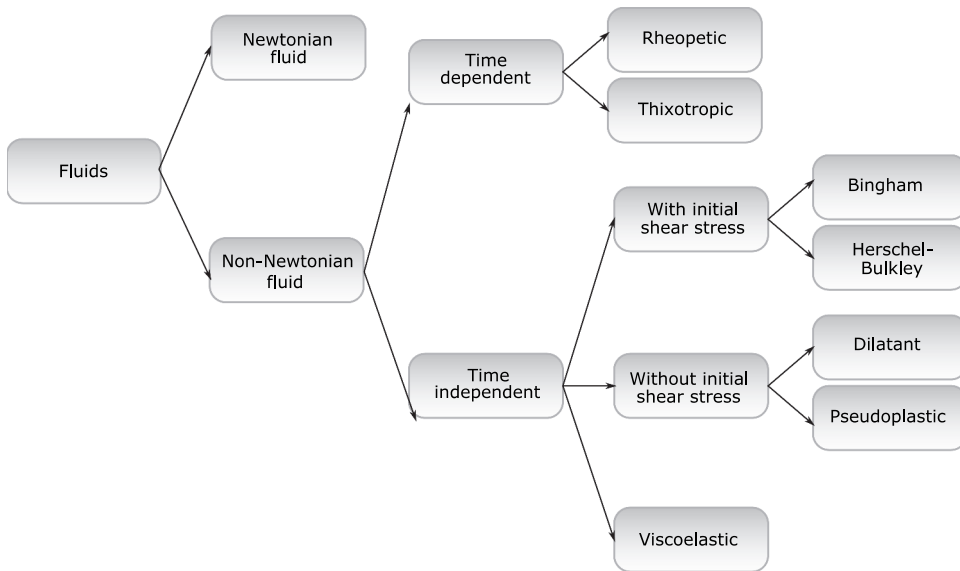


**Figure 3.** Classification of fluids in rheology behaviours.

Fluids can be classified into two main categories, Newtonian and Non-Newtonian fluids. In simple terms, the viscosity of Newtonian fluids is not dependent on the shear rate and these fluids present a linear correlation between the shear rate and the shear stress. While the Non-Newtonian fluids have non-linear relationship between the shear rate and the shear stress and their viscosity is dependent on the shear rate, their viscosity can also be time-dependent. The fluids classification is shown in [Figure 3](#).

The rheology of structural adhesives can be confused sometimes; the variability in viscosity is caused by chemical reactions between the components, so it is not classified as a rheopetic fluid. The rheopetic fluid changes viscosity due to shear stress and the fluid can recover its initial behaviour. In order to determine the rheological behaviour of an adhesive, rheological tests are necessary to measure viscosity during the application of shear stress. Commonly referenced rheologically significant behaviours obtained from experimental squeeze tests are listed in [Table 1](#). Improvements to these models may could be necessary to represent some specific fluid flows in the case of viscoelastic behaviour, for example .<sup>[8,26]</sup>

### **2.3. Interest in simulating the adhesive squeeze**

Interest in the study of the squeeze flow is common in various application domains. One recent example is in the field of disassembly on demand (DoD), in which the interest is to study and optimize the spreading of an adhesive with encapsulated agents or nanoparticles. In this case, studies of the squeeze in



**Table 1.** Synthesis of the rheological behaviour and its responses under squeeze mode.

Rheological behaviour	Main characteristic <sup>[19–21]</sup>	References	Examples <sup>[20]</sup>
Newtonian fluid	Its viscosity is not dependent on shear rate	[22–25]	Water, alcohol, blood plasma
Rheopectic	The viscosity increases with time that it remains under shear stress and it can be called time-dependent dilatants	-	Printer inks, gypsum pastes
Thixotropic	In this case, the viscosity decreases with the time that it remains under shear stress and it can be called time-dependent pseudoplastics	[26,27]	Yoghurt, gelatine gels
Bingham	Presents a linear relationship between shear stress and shear rate and needs initial yield stress before it begins to flow	[23,28–31]	Toothpaste, mayonnaise,
Herschel-Bulkley	Behaviour similar to a pseudoplastic fluid, but with an initial yield stress	[8,32–35]	Ordinary paints
Dilatant (Shear-thinning)	Increase in apparent viscosity as the shear rate increases and do not needs minimum shear stress to start to flow	[36–38]	Quicksand, cornflour in
Pseudoplastic (Shear-thinning)	The viscosity decreases with increasing stress and does not needs minimum shear stress to start to flow	[37]	Ketchup, blood, nail polish
Viscoelastic	Fluids that exhibit both viscous and elastic characteristics when submitted a some load	[39]	Blend of a solvent and some polymer

a particulate flow<sup>[22,40–42]</sup> can be a good starting point. Another solution is to consider similar problems in other scientific fields, such as the displacement of marine specimens overtime knowing the initial position<sup>[43,44]</sup>, the movement of fresh concrete<sup>[45–47]</sup>, or volcanic lava flow<sup>[48,49]</sup>. Besides applications in the assembly domain, the squeeze flow theory can be applied to study soft solid behaviour, with the hypothesis that movement can be compared to a viscous fluid<sup>[8,23,26]</sup>. Squeeze is also applied in classical problems, such as the simulation of lubrication films and their behaviour under different external conditions and geometries<sup>[32,50,51]</sup>. Furthermore, among applications outside of this engineering domain, the food sector uses the squeeze flow theory extensively<sup>[52,53]</sup>.

Specifically in this work, the interest is to describe the numerical models that can be applied to study adhesive squeeze during the assembly process. As shown in<sup>[28]</sup>, the cover surface and overflowing adhesive are important variables in cases where thickness is fixed. In<sup>[28,54]</sup> the authors took an interest in validating the final form after the assembly process, including the surface covered and overflowing adhesive using Computational Fluid Dynamics (CFD). In the case presented in,<sup>[55]</sup> the authors study the adhesive flow, but here to study the impact of the deposition process with the application of two adhesive cords.

For the simulation of the adhesive squeeze, another important aspect is the discretization schemes, in terms of time and space, because of the impact on the numerical method to be applied. Among the methods presented in the literature, the grid-based numerical methods are widely used for fluid simulations, either using the Lagrangian or Eulerian reference frame, including the finite difference method (FDM), finite volume method (FVM), or the finite

element method (FEM) [56]. In this study, the Smooth Particle Hydrodynamics (SPH) method will also be considered. This is a meshfree method associated with particulate discretization of the matter and the movement [57].

### 3. DISCRETIZATION AND APPROXIMATION METHODS

The numerical solution of time-dependent conservation equations, in a Lagrangian or an Eulerian description, requires their discretization in time and space. There are different approaches to each of these components, the fundamentals of which will be described here. The objective of this section is to analyse the relevance of discretization methods and the set of conservation equations related to its application for squeeze flow simulation. It is important to note that most of the simulations are time-dependent. The time discretization method is implicitly related to the choice of the numerical method used to describe the deformation of the adhesives.

#### 3.1. Conservation equations

In order to understand and describe the behaviour of the adhesive's highly deformable dynamics in its non-polymerized state, it is necessary to take into account three conditions: conservation of mass, conservation of momentum, and conservation of energy. The development of the conservation equations for both forms can be consulted in [58] and the final expressions for the Lagrangian description are presented in Table 2 and Table 3 for the Eulerian description.

The continuity equation represents the mass conservation of the system. The  $\rho$  is the density of the fluid and it can be depend on direction and time and  $V$  represents the velocity vector field in Cartesian space given by

**Table 2.** Conservation equations for the Lagrangian description.

Continuity	$\frac{\partial \rho}{\partial t} + \rho \cdot \nabla = 0$
Momentum	$\rho \frac{Du}{Dt} = -\frac{\partial p}{\partial x} + \frac{\partial \tau_{xx}}{\partial x} + \frac{\partial \tau_{yx}}{\partial y} + \frac{\partial \tau_{zx}}{\partial z} + \rho f_x$
	$\rho \frac{Dv}{Dt} = -\frac{\partial p}{\partial y} + \frac{\partial \tau_{xy}}{\partial x} + \frac{\partial \tau_{yy}}{\partial y} + \frac{\partial \tau_{zy}}{\partial z} + \rho f_y$
	$\rho \frac{Dw}{Dt} = -\frac{\partial p}{\partial z} + \frac{\partial \tau_{xz}}{\partial x} + \frac{\partial \tau_{yz}}{\partial y} + \frac{\partial \tau_{zz}}{\partial z} + \rho f_z$
Energy	$\rho \frac{D}{Dt} \left( e + \frac{V^2}{2} \right) = \rho \dot{q} + \frac{\partial}{\partial x} \left( k \frac{\partial T}{\partial x} \right) + \frac{\partial}{\partial y} \left( k \frac{\partial T}{\partial y} \right) + \frac{\partial}{\partial z} \left( k \frac{\partial T}{\partial z} \right) - \frac{\partial (up)}{\partial x}$ $- \frac{\partial (vp)}{\partial y} - \frac{\partial (wp)}{\partial z} + \frac{\partial (u\tau_{xx})}{\partial x} + \frac{\partial (u\tau_{yx})}{\partial y} + \frac{\partial (u\tau_{zx})}{\partial z} + \frac{\partial (v\tau_{xy})}{\partial x} + \frac{\partial (v\tau_{yy})}{\partial y}$ $+ \frac{\partial (v\tau_{zy})}{\partial z} + \frac{\partial (w\tau_{xz})}{\partial x} + \frac{\partial (w\tau_{yz})}{\partial y} + \frac{\partial (w\tau_{zz})}{\partial z} + \rho f \cdot V$

**Table 3.** Conservation equations for the Eulerian description.

Continuity	$\frac{\partial \rho}{\partial t} + \nabla \cdot (\rho \mathbf{V}) = 0$
Momentum	$\frac{\partial (\rho u)}{\partial t} + \nabla \cdot (\rho u \mathbf{V}) = -\frac{\partial p}{\partial x} + \frac{\partial \tau_{xx}}{\partial x} + \frac{\partial \tau_{yx}}{\partial y} + \frac{\partial \tau_{zx}}{\partial z} + \rho f_x$
	$\frac{\partial (\rho v)}{\partial t} + \nabla \cdot (\rho v \mathbf{V}) = -\frac{\partial p}{\partial y} + \frac{\partial \tau_{xy}}{\partial x} + \frac{\partial \tau_{yy}}{\partial y} + \frac{\partial \tau_{zy}}{\partial z} + \rho f_y$
	$\frac{\partial (\rho w)}{\partial t} + \nabla \cdot (\rho w \mathbf{V}) = -\frac{\partial p}{\partial z} + \frac{\partial \tau_{xz}}{\partial x} + \frac{\partial \tau_{yz}}{\partial y} + \frac{\partial \tau_{zz}}{\partial z} + \rho f_z$
Energy	$\frac{\partial}{\partial t} \left[ \rho \left( e + \frac{V^2}{2} \right) \right] + \left[ \rho \left( e + \frac{V^2}{2} \right) \mathbf{V} \right] = \rho \dot{q} + \frac{\partial}{\partial x} \left( k \frac{\partial T}{\partial x} \right) + \frac{\partial}{\partial y} \left( k \frac{\partial T}{\partial y} \right)$ $+ \frac{\partial}{\partial z} \left( k \frac{\partial T}{\partial z} \right) - \frac{\partial (up)}{\partial x} - \frac{\partial (vp)}{\partial y} - \frac{\partial (wp)}{\partial z} + \frac{\partial (u\tau_{xx})}{\partial x} + \frac{\partial (v\tau_{yx})}{\partial y} + \frac{\partial (w\tau_{zx})}{\partial z}$ $+ \frac{\partial (v\tau_{xy})}{\partial x} + \frac{\partial (v\tau_{yy})}{\partial y} + \frac{\partial (v\tau_{zy})}{\partial z} + \frac{\partial (w\tau_{xz})}{\partial x} + \frac{\partial (w\tau_{yz})}{\partial y} + \frac{\partial (w\tau_{zz})}{\partial z} + \rho \mathbf{f} \cdot \mathbf{V}$

$$\mathbf{V} = u\mathbf{i} + v\mathbf{j} + w\mathbf{k} \quad (1)$$

Meanwhile, the momentum conservation equation applies the physical principle of Newton's second law to the system. The forces responsible for the fluid movements have two sources: surface forces (first term on the right side) and body forces (second term on the right side). The surface forces act on the surface of the fluid element and are represented by the contribution of pressure ( $p$ ) and shear stress ( $\tau$ ) exercised. Secondly, the body forces act on the volumetric mass of the fluid element and  $f$  is this force per unit mass in each direction.

The last equation represents energy conservation in terms of total energy  $e + V^2/2$ , where  $\dot{q}$  represents the heat flux,  $T$  is the temperature,  $k$  the thermal conductivity and the term  $\rho \mathbf{f} \cdot \mathbf{V}$  is the rate of work done by the body force acting on the fluid element moving at a velocity  $\mathbf{V}$ .

### 3.2. Space discretization

The differential equations are applied in several domains and consequently there are many numerical methods to the resolution described in the literature. These methods differ according to the discretization of the spatial derivatives of the differential equations. They are traditionally classified in Eulerian methods, Lagrangian methods, alongside the Arbitrary Lagrangian Eulerian methods [58].

In short, the differences between the discretization methods are related to the mesh characteristics. The first and most used, the Eulerian description (see [Figure 4a](#)), is represented by a grid fixed in the space and the material moves inside the grid. As a result, the material deformation depends on the disposition and size of this fixed grid. These methods, in general, are more stable and can represent material deformations without change to the grid. But the major disadvantages are (i) the difficulty of representing domains with a complex

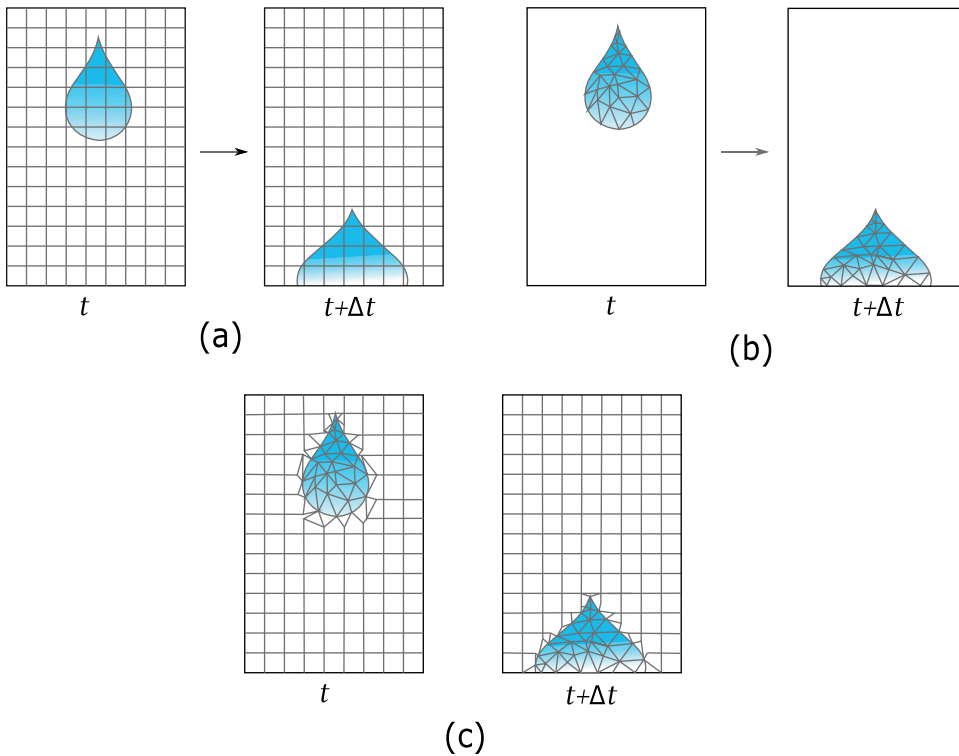


**Figure 4.** Representation of space discretization. (a) Eulerian description, (b) Lagrangian description, (c) Arbitrary Lagrangian Eulerian description.

geometry in a regular grid, (ii) the capture of the fluid-free surface having a defined relevant interface and (iii) high memory storage<sup>[59]</sup>. In this situation, the slip/stick condition of the material on the substrate is represented through its ability to resist shear in a thin layer at the vicinity of the wall<sup>[2,15]</sup>.

The Lagrangian description (see Figure 4b) is a method with the grid placed inside the material and the deformation of this is caused by the mesh deformation. Consequently, accuracy depends on the grid size and distribution. A particular class among the methods with Lagrangian descriptions is the meshfree method, which uses a finite number of particles for the discrete state and dynamics of a material<sup>[59]</sup>. The main advantages of grid-based Lagrangian methods include no extra computational effort to calculate the convective (or advective) terms. The convective term is zero because the boundary control volume is coincident with the boundary of a control mass<sup>[60]</sup>. Since the mesh is not fixed in space, the complex geometries are easily discretized and the mesh involves only the computational domain where material exists. Nevertheless, these methods present some difficulties in representing materials with large deformations. On the other hand, the meshfree Lagrangian methods have as advantages, compared to the grid-based methods,

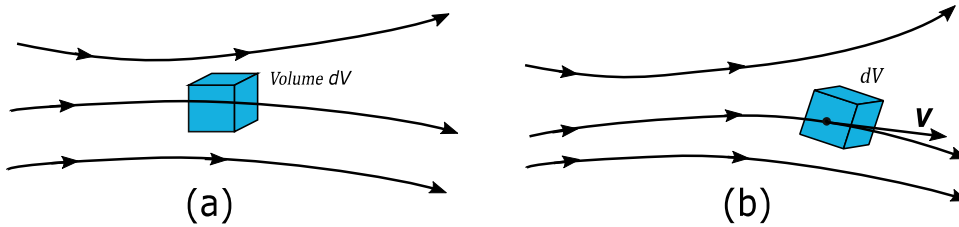


**Figure 5.** Representation of an infinitesimal fluid element fixed in space (a) and moving along a streamline (b).

their facility to represent the material by a system of particles without fixed node connectivity. This approach is therefore better suited to representing large deformations <sup>[59]</sup>.

The arbitrary Lagrangian–Eulerian (ALE) description was developed in an attempt to combine the advantages of the above classic kinematical descriptions while minimizing their respective drawbacks insofar as possible. In the ALE description, the nodes of the computational mesh may be moved with the continuum in normal Lagrangian fashion, or be held fixed in an Eulerian manner (see Figure 4c), or be moved in some arbitrarily specified way to give continuous rezoning capability <sup>[61]</sup>.

In general, the governing equations for representing the fluid can be separated into two categories: conservative form, when the infinitesimal fluid element is fixed in space and only the fluid moves (see Figure 5a), and the non-conservative form, when the infinitesimal fluid element moves in the same fluid velocity (see Figure 5b).

The choice of the description used and space description is based on the objective to be achieved and the limitations. In general terms, Lagrangian discretization is used to observe fluid movement through space and time, for example, in order to study wave propagation. The Eulerian description is very useful for observing a specific point in space.

#### 4. NUMERICAL MODELLING METHODS

Grid-based methods, like finite elements of finite volumes, are traditionally the most common in the literature for fluid and solid simulations. Despite their popularity and wide usage, they still present limitations in some cases, for example for large deformations or crack generation and propagation modelling. In such cases, meshfree methods are good alternatives. Advantages and limitations, as well general aspects of each method, are presented in the next sections, keeping in mind the application case for predicting adhesive distribution during and after bonding.

## 4.1. Grid-based methods

So called grid-based methods are tessellation methods for discretizing the medium. Tessellation is composed of elements which are plain parts of matter and nodes which are the connections between the elements. The behaviour of the matter is described by kinematic data at nodes (displacement, velocity, acceleration), and by internal state variables usually in a tensor form (stresses, strains, energy, pressure, etc.). The tessellation, or mesh, can be structured (composed of rectangular zoning) or unstructured (free arrangement of elements), composed on rectangular (or parallelepipeds) or triangular (or prisms, pyramids) elements.

### 4.1.1. Finite Difference Method (FDM)

Figure 6 presents the adhesive in a structured grid in its initial position before spreading. The grid is structured and boundaries of each element are straight lines that are aligned. Each grid node may be considered as the origin of a local coordinate system whose axes coincide with the grid lines (see Figure 6).

Each node is uniquely identified by a set of indices that are the indices of the grid lines that intersect at it,  $(i, j)$  in 2D and  $(i, j, k)$  in 3D. In general terms, this method uses the Taylor expansion series to solve the problem at a discrete point with precision related directly to the order of the Taylor series.

Using this expansions method, it is possible to obtain approximate expressions for the first and higher derivatives at point  $x_i$  in terms of the function values at neighbouring points using central, forward and backward schemes. Figure 7 shows the graphical representation of each approximation method.

In this case, the error is due to the truncation of the Taylor series, which is called the truncation error, as well as with the discretization applied for the approximation or with the scheme chosen for the finite difference

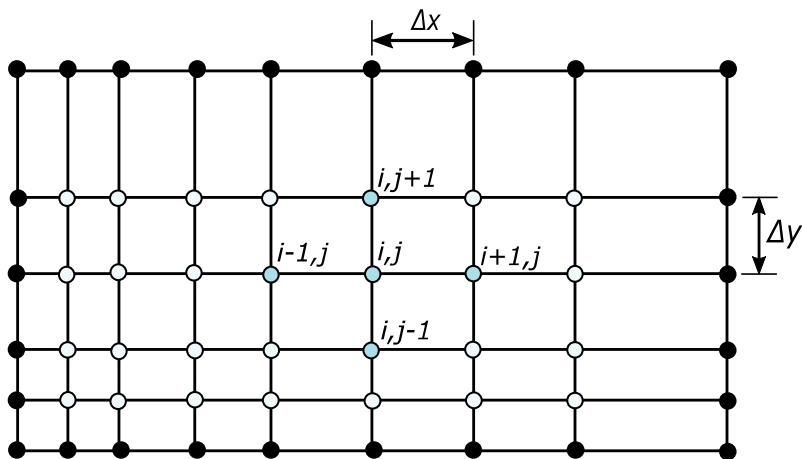
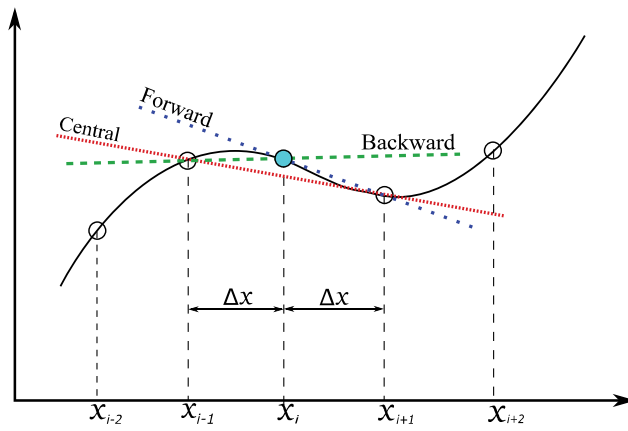


Figure 6. 2D Cartesian grid for finite differences methods.



**Figure 7.** Geometric interpretation of the approximation of first-order derivatives.

approximations <sup>[60]</sup>. Because of its formulation, the FDM is a very precise method, which means that the results from this type of approximation can be very close to the exact solution, providing the size of the mesh discretization is convenient (small enough, but not too small to avoid non-useful computations) <sup>[62]</sup>.

One important application of the finite difference method in the fields of fluid simulations is the simulation of film lubrication <sup>[50]</sup>. The partially filled gaps (PFG) method is particularly interesting to observe the interaction between the interfaces and the flow. This method can also be used in the adhesion domain to study the compression effect in the adhesive. <sup>[63]</sup> Another advantage of the FDM is the possibility to represent slippage; in <sup>[33]</sup>, the author presents an approximation of the shape of the yield surface, the velocity and stress fields between two circular plates.

#### **4.1.2. Finite Volume Method (FVM)**

The finite volume method is a discretization method that is well suited to various types of numerical simulation (elliptic, parabolic or hyperbolic, for instance) of conservation laws. This method has been extensively used in several engineering fields, such as fluid mechanics, and heat and mass transfer <sup>[64]</sup> in the petroleum, aerospace, automotive industry. Consider the generic conservation equation for a scalar quantity  $\phi$  and assume that the velocity field and all fluid properties are known. Consider also an arbitrary control volume (CV) in the space through which the fluid flows with a geometrical contour called the control surface (S).

The FVM begins with the integral form of an equation divided into two parts: one related to the calculation on the surface S, and another related to the control volume CV, represented by integration in the control volume.

$$\int_S (\rho \phi \vec{u}) \cdot \vec{n} dS = \int_S (\Gamma \text{grad} \phi) \cdot \vec{n} dS + \int_{CV} q_\phi dV \quad (2)$$

where  $\rho$  is the flow density,  $\vec{u}$  the velocity vector and  $\vec{n}$  the normal vector to the surface control.

It is possible to find the solution to this equation by using approximations of the domain's subdivision into a finite number of small control volumes with defining boundaries. The most common and simplest method to solve the integral in the control volume is to use the middle point P and its Cartesian representation as shown in [Figure 8](#).

$$\int_{CV} q_\phi dV \approx q_P \text{Vol}(CV) \quad (3)$$

where  $q_P$  the value of  $q$  at the CV centre. This approximation is exact if  $q$  is either constant or varies linearly within the CV.

To solve the integrals for the surface; the net flux through the CV boundary is the sum of integrals over the faces:

$$\int_S f \cdot \vec{n} dS = \sum_k \int_{S_k} f dS \quad (4)$$

where  $f$  can assume the term of convective flux ( $f^{conv} = (\rho \phi \vec{u}) \cdot \vec{n}$ ) or diffusive flux ( $f^{diff} = (\Gamma \text{grad} \phi) \cdot \vec{n}$ ).

In the approximation of this integral calculated using the points of the control volume, the accuracy and order of error depend directly on the interpolation chosen. For example, for the midpoint rule, the only point used is the central point of the surface,  $e$  on the east face (see [Figure 8](#)) and it will generate an error of order 2. If the Simpson's rule is used, however, three

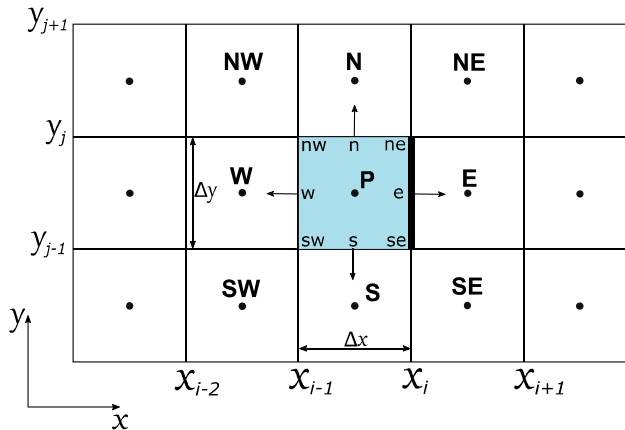


**Figure 8.** 2D Cartesian grid for finite volumes methods.



points of the surface will be necessary,  $ne$ ,  $e$  and  $se$  on the east face, and in this case, the error is of order 4 <sup>[60]</sup>. Another error source is related to the approximations used to calculate  $\phi$  to obtain flux values,  $f^{conv}$  and  $f^{diff}$ .

In general, the FVM is the most widely used in the field of fluid analysis, the principal of which was presented in this section. Among the examples of application, some are more interesting for use as an example for the adhesive's squeeze flow.

First, there are the models used to represent injection and moulding, overall, these studies look into the final form after the demoulding and into the internal stress generated during the injection process. In this type of application, the velocity of injection plays an important role in the process, so the transient regime is also studied <sup>[65–67]</sup>.

Another aspect discussed by many authors is the fluid behaviour representation that can be exploited with two approaches: Newtonian and non-Newtonian behaviour, which can be done with an analytical method or numerical simulations. The choice between these two methods depends on the hypothesis considered; the accuracy level and the geometry of the study, for example. The analytical method is used for simple geometries (flat plates, for example) and non-complex fluid behaviour (without dependency on other parameters, for example) <sup>[11,23,29,32,34]</sup>. In the majority of cases, an analytic method cannot solve the question and the numerical simulation is applied <sup>[28,45,46,54,63,68]</sup>.

#### **4.1.3. Finite Element Methods (FEM)**

The finite element method, like the finite volume method, cuts a structure into small elements connected by common nodes. The distinguishing feature between the finite element method and the finite volume method is that with the finite element method, equations are multiplied by a weight function before being integrated over the entire domain. The formulation and particularities can be consulted in <sup>[18]</sup>. The conditions applied to the nodes shared by two or more elements guarantee the continuity of the displacement solution across finite element boundaries. The general idea is to solve the Navier-Stokes equations for each element using an approximation by shape function. The formulation and implementation of this methodology for Navier-Stokes equations can be found in classical works <sup>[18,69–71]</sup>.

The main inconvenience of the finite element method with an Eulerian approach is to solve problems with extreme deformations. As shown in section 2.2, fluid movement in this type of discretization is extremely dependent on the size of the elements chosen. In cases where the displacement is large, one of the most common errors is stretching the elements until element failure. The solution is a combination of both discretization, Lagrangian and Eulerian, with a mesh with automatic and continuous rezoning of the fluid mesh <sup>[72–74]</sup>. The

finite element is not the method most commonly used for fluid analysis, but it can be an interesting method for studying cases with an incompressible viscous fluid flow <sup>[75-79]</sup>.

Lagrangian Finite Element models can also be found in the literature to analyse the behaviour of other solid-like fluids such as shear-thickening fluids (STF) <sup>[80,81]</sup>. A reason why Lagrangian Finite Element models can be preferable is because the fluid's viscous resistance becomes very high and significant, compared to the compressible one. This paper is not concerned with this case of materials, but it seems important to point out that there may be some similarities in the material behaviour descriptions, such as the use of the solid-like Johnson-Cook material model <sup>[36]</sup>.

#### **4.2. Meshfree methods for fluid simulations**

A meshfree particle method (MPM) in general refers to the class of meshfree methods that employ a set of a finite number of discrete particles to represent the matter (fluid in this case) and its movement. Each particle can either be directly associated with one discrete physical object or be generated to represent a part of the continuum problem domain <sup>[82]</sup>. The analysis is focused on the Smoothed Hydrodynamic Particles (SPH) method.

Among the meshfree methods that exist in the literature, Smoothed Particles Hydrodynamics (SPH) is the most commonly used in fluid applications. Proposed in 1977 by Gingold and Monaghan <sup>[83]</sup> and Lucy <sup>[84]</sup>, initially for solid applications, it was adapted for fluid mechanics a few years later, also by Gingold and Monaghan <sup>[85]</sup>. This method is of particular interest in fluid-structure interaction simulation (FSI), even in situations where surface tensions and wetting effects are to be taken into account <sup>[57]</sup>.

The SPH is an explicit Lagrangian particle method based on an interpolation theory. The conservation laws of fluid dynamics (Table 2) are converted into integral equations. The value of a specific particle  $i$  is approximated from the function values for surrounding particles in the influence domain of particle  $i$  <sup>[86]</sup>. In simple terms, all the particles inside the influence area have a contribution to the particle of interest and the importance of this contribution depends on their distance in relation to this particle (see Figure 9).

Approximation of a function  $f(x)$  used in the SPH method is based on the smoothing function, also called the kernel function. The method starts with an integral based on the Dirac delta function, which cannot be used for establishing discrete numerical models. To solve this, the Delta function must be replaced with the kernel function.

$$\langle f(x) \rangle = \int_{\Omega} f(x') W(x - x', h) dx' \quad (5)$$

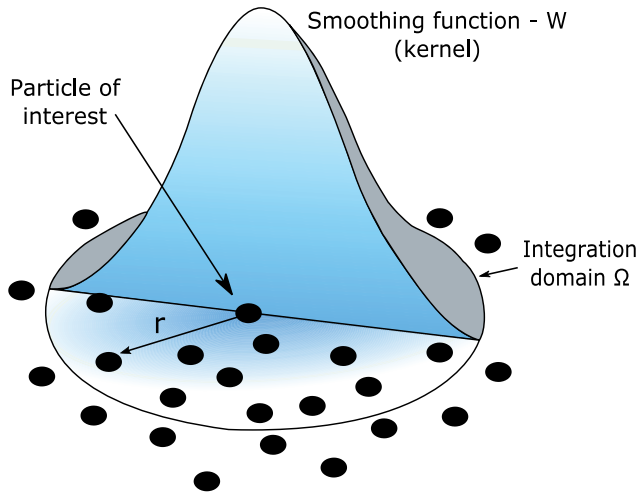


**Figure 9.** Graphic representation of the kernel function.

where  $f(x)$  is defined and continuous in the integration domain  $\Omega$ . The  $h$  is the smoothing length defining the influence or support area of smoothing function  $W$  and  $x$  is the particle distance.

Succinctly, the kernel function must satisfy three conditions: the normalization condition, the delta function property that is observed when the smoothing length approaches zero, and the compact condition. These conditions are described in Table 4, where  $\kappa$  is a constant related to the smoothing function for a particle at  $x$ .

After the discretization process applied to the continuous domain in  $N$  particles, each having its mass and physical properties, the continuous form of kernel approximation expressed in Eq. (5) can be written in the discretized form of a summation of the neighbouring particles as follows:

$$\langle f(x) \rangle = \sum_{j=1}^N \frac{m_j}{\rho_j} f(x_j) W(x - x_j, h) \quad (6)$$

where  $\rho_j$  is the density of particle  $j$ .

As shown in Figure 10, each particle inside the influence ratio influences particle  $j$  of interest and that level of influence depends on the distance at particle  $j$ . Each particle of the domain has its influence area and it moves with the particle movement. In conclusion, the same particle can be part of many influence areas.

**Table 4.** Conditions for the kernel function.

Normalization condition	$\int_{\Omega} W(x - x', h) dx' = 1$
Delta function property	$\lim_{h \rightarrow 0} W(x - x', h) = \delta(x - x')$
Compact condition	$W(x - x', h) = 0$ when $ x - x'  > \kappa h$

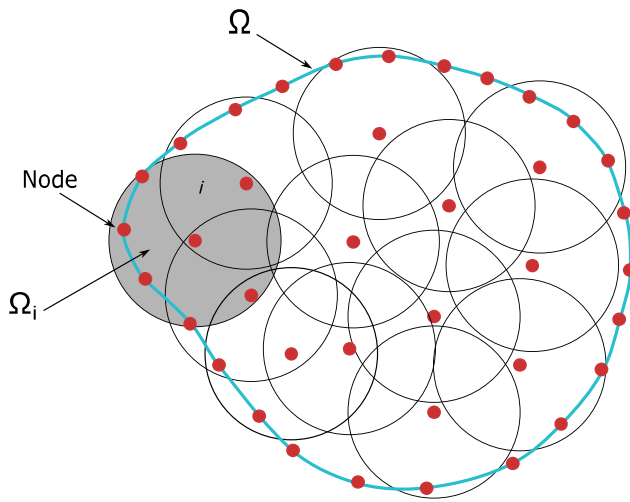


**Figure 10.** Graphic representation of influence areas.

A particularity of this method is the difficulty in dealing with borders because the influence areas exceed the principal shape and there are no particles in this place. One solution for this problem is the creation of ghost particles without physical properties and with null influence.

This method's Lagrangian formulation and its discretization form makes the SPH the most commonly used method for applications with solids in fast dynamics, explosions, high-speed impacts, etc. Examples of the application of this method and formulation with details can be consulted in [56,87,88].

Even though the SPH was not specifically developed specifically for fluid simulations, there are many studies on this field in the literature. The first class of studies is dedicated to improving border conditions, which means proposing other solutions for representing and calculating the fluid's free surface [89–92]. In the category of fluid behaviour, the SPH is used to simulate incompressible [93] and compressible fluids [94], besides that the method offers the capability of calculating multi-fluid interactions [95,96] or fluid-structure interaction [97]. Another highly interesting application for this methodology in the computational graphics field is the possibility to predict the fluid's movement and final form [98,99].

### **4.3. Comparison between numerical methods**

The objective of this section is to present a comparison between the previously described methods based on parameters that are important for simulating the spreading process.

First, the FDM is a very interesting method for studying simple aspects of flow, as shown in the examples presented previously in this paper. Besides that, the error of approximation can be minimized by reducing the size of the discretization to infinitesimal elements though increasing the time calculation and computational effort. While the FVM is an improvement on the previous method, the main characteristic is the subdivision of the domain into a finite number of control volumes. As with the FDM, the FVM does not generally presents instabilities or convergence problems for ensuring the law of conservation within each control volume. On the other hand, to ensure a good representation of the fluid movement and minimum error, discretization must be very thin and the problem is the same as with the FDM.

The FEM is considered a boundary conditions method. Contrary to FVM, elements in the FEM are composed of many nodes (dependent on the element chosen) and the error can be reduced using a high-degree approximation. However, as presented in [section 4](#) “Discretization and approximation methods”, the classical FEM used for structural applications is not adapted to fluid analysis and the method needs to be updated for approximation, space discretization, etc. Even if this update method is already capable of simulating incompressible flows and injections, the updates made in order to represent these behaviours increase the computation resources necessary.

In the end, the SPH can be a powerful resource for fluid simulations, especially for adhesive squeeze, once displacement is not coupled with mesh size. The advantage of this method lies in representing large deformations. This method’s application is still in its infancy, however, so many updates are still needed, for example, in the implementation of the behaviour laws for non-Newtonian fluids, and improvements on the methods used to represent the free surface.

After studying the main characteristics, advantages and limitations of these numerical methods, it is possible to compare these methods based on the maturity of the method in describing certain major parameters for the adhesive squeeze. This comparison is presented in [Table 5](#), where the parameters are separated into two categories: adhesives and substrates, and each parameter received a score between a one and three plus symbol. One represents low maturity, i.e. it needs several updates, and three means that the method is already well consolidated.

**Table 5.** Comparison of the maturity of numerical methods.

Capabilities		FDM	FVM	FEM	SPH
ADHESIVE	Thickness	+++	+++	+++	++
	Adhesive behaviour	+++	+++	++	++
	Final form	+++	+++	++	+
	Initial distribution	+++	+++	+++	+++
SUBSTRATE	Deformability	-	-	+++	+++
	Curvature	+	-	+++	+++
	Slid	+++	+++	++	++
	Roughness	+	+	+++	+++
	Approach condition	++	++	+++	+++

One strategy that can be applied when a method is not able to simulate certain characteristics to couple two methods, for example, is the deformability of the substrate or roughness [100,101].

## 5. APPLICATION

As discussed in the previous sections, adhesive squeeze can follow various approaches depending on desired final results. In this specific case, the interest lies in studying feasibility to represent the adhesive as a smooth solid, i.e. representing the adhesive using a soft solid behaviour law with weak properties, with SPH. For this preliminary study of parameter influences, the output is the size and shape of the adhesive's recovery area on the substrate, which will be compared with preliminaries experimental results.

### 5.1. Experimental testing

The experimental testing was carried out in the interest of observing the adhesive distribution during and after spreading imitating the bonding process. Due to the difficulty of visualization, the tests were realized outside of standard tensile machines with a home develop weight system. A representation of the experimental setup is shown in Figure 11a. The spreading system is composed of a flat  $150 \times 100 \text{ mm}^2$  aluminium fix plate (bottom) with a non-controlled surface roughness on which two  $34 \times 17 \text{ mm}^2$

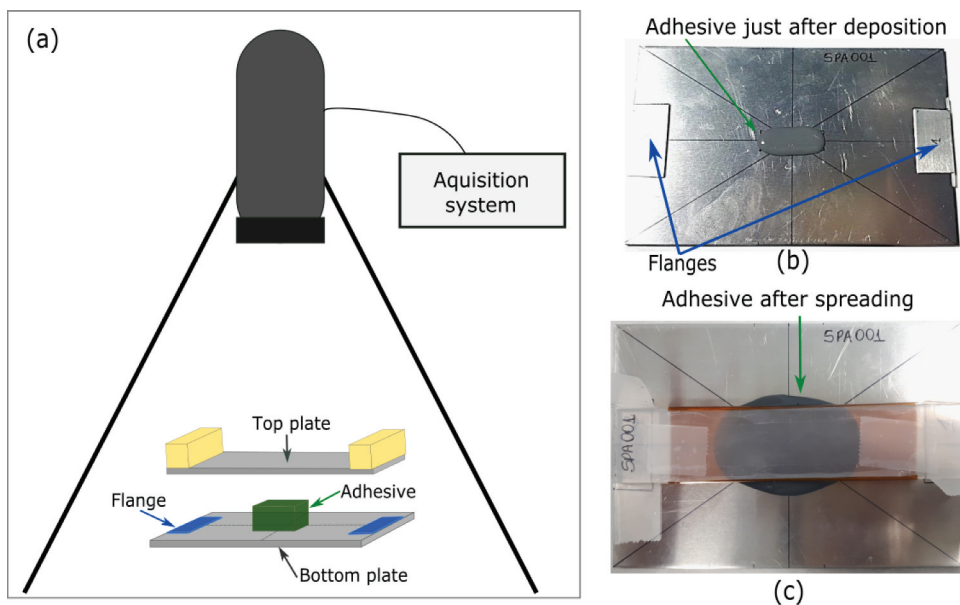


**Figure 11.** Experimental set up for spreading tests (a); top view of adhesive distribution before (b) and after (c) testing.

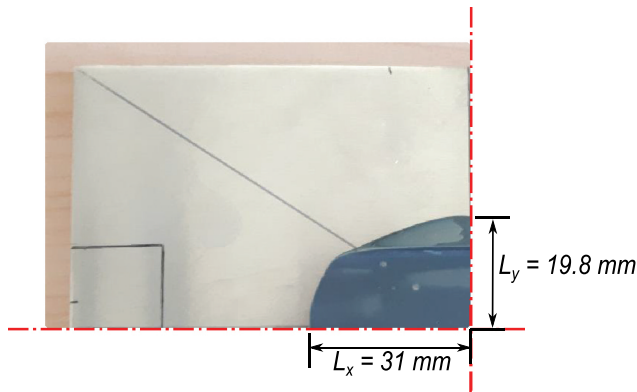


**Figure 12.** Experimental parameters used as reference for sensitivity study.

aluminium flanges of 1.2 mm thickness each are fixed symmetrically to ensure the final thickness of the bonded joint. The adhesive is deposited at the middle of the bottom plate upper face and its initial geometry is shaped like a parallelepiped (Figure 11b). The loading consists of two metallic blocks of 250 g each placed at the extremities of a 150x30x20mm<sup>3</sup> Plexiglas beam and submitted to gravity. The Plexiglas beam is covered by a transparent non-sticking film of 0.1 mm thickness (Figure 11c) to allow both the video recording of the adhesive spreading during squeezing through it, and separation with the adhesive after curing (7 days at room temperature).

An Ultra High-Speed Camera Photron 5A5 is placed above the complete system and takes pictures at 125fps. It is possible then to measure the spreading of the adhesive during bonding from top view (Figure 12), and to observe the qualitative 3D shape during and after the bonding process. If a squeeze out pudding with a cylindrical shape has been observed during bonding as can be found in the literature <sup>[54]</sup>, the final shape of the adhesive at the Plexiglas boundary is a meniscus. This is due to the high deformability of the non-cured EC2216 which does not keep its round shape, immediately obtained during bonding because of its incompressibility. For comparison with numerical results, the two characteristic lengths were considered,  $L_x$  being the length along the length of the upper substrate and  $L_y$  the length in the direction of the width of the upper substrate (see Figure 12), along with the general shape including the corner format.

## **5.2. Numerical model using SPH**

Fluid simulation is usually done using CFD codes, but as discussed in the previous sections, setting models is not easy. Fluid characterisation for determining behaviour law coefficients requires an extensive experimental

campaign. Among the principal tests, measuring viscosity is particularly problematic because it is directly dependent on fluid behaviour. In this context, the objective is to simplify the numerical simulation of the adhesive squeeze and to obtain a model that takes a minimum of experimental tests and provides the final form of the adhesive. For that purpose we have decided to use a solid mechanics solver, LS-DYNA®, and model the adhesive using the Lagrangian Smooth Particle Hydrodynamics (SPH) method with stress-strain behaviour laws that allow taking in consideration both shear and bulk resistances. The model is developed to reproduce the experimental set-up. To reduce the computational cost, the problem was considered symmetrical, and the model considers only a quarter of the structure (Figure 13). All components except the adhesive are modelled using non-deformable finite elements. The bottom plate is fixed in space as well as the flanges. The Plexiglas beam is allowed to move vertically. A penalty contact method without friction is chosen to manage the contact between the all components with the adhesive. The adhesive is modelled using 20,000 SPH particles with a uniform distance between particle of 0.3 mm.

The adhesive was described as a smooth solid represented by Johnson-Cook behaviour law (Eq. (7))<sup>[102]</sup> coupled with Murnaghan equation of state (Eq. (8))<sup>[102]</sup>.

$$\sigma_y = (A + B\bar{\epsilon}^n)(1 + c \ln \dot{\epsilon}^*) \left( 1 - \left( \frac{T - T_{room}}{T_{melt} - T_{room}} \right)^m \right) \quad (7)$$

$$p = k_0 \left( \left( \frac{\rho}{\rho_0} \right)^\gamma - 1 \right) \quad (8)$$

In Eq. (7),  $A$ ,  $B$ ,  $c$ ,  $n$ , and  $m$  are input constants to be determined,  $\bar{\epsilon}^p$  is the effective plastic strain,  $\dot{\epsilon}^*$  is the normalized effective plastic strain rate and  $T_{room}$  and  $T_{melt}$  represent the room and melt temperature, respectively, while in Eq. (8),  $k_0$  and  $\gamma$  are input constants to be determined, and  $\rho$  is the adhesive density.

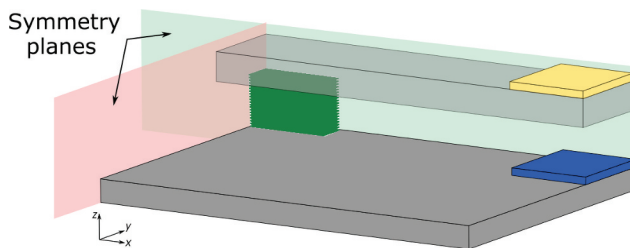


**Figure 13.** Schematisation of the numerical model.



The Johnson-Cook law can be used to separate the evolution of the yield stress as a function of three behaviours, plastic hardening, the effect of strain rate and the temperature effect. As these effects are uncoupled, their combination provides the adhesive representation. First, the temperature effect is also studied, but its impact is less important than the other two behaviours in the final adhesive form, considering the melt temperature as high enough not to melt the material during the process. The Murnaghan equation of state is a relationship between the volume of a body and the pressure to which it is subjected, considering an incompressible behaviour. So after disregarding the temperature effect, the elastic-plastic behaviour and the effect of the strain rate remain to be studied. The next section focuses on a sensitivity analysis of the parameters related to these behaviours.

### 5.3. Sensitivity analysis

The sensitivity analysis consists here in varying each parameter of the Johnson-Cook behaviour law and of the Murnaghan equation of state (EOS), considering a reference case. The reference values presented in Table 6 were chosen as the mean values of data extracted from a preliminary bibliographic analysis. The bibliographic analysis was also used to define the variation range for each parameter or property. The following sections present the results of the variation study.

#### 5.3.1. Influence of compressibility

It can be concluded that the equation of state has considerable influence on both lengths of reference ( $L_x$  and  $L_y$ ). As shown in Figure 14 and Figure 15, both parameters have similar influence. The variation of these parameters changes the lengths in x and y, but the modification in the corner is the only result of these changes, with no direct modification related to these parameters. Another interesting aspect is the evolution of the reference values with the parameters of the EOS. In both cases, the lengths present a maximum value that then starts to decrease. Moreover, small values in both cases can induce numerical instabilities. This error is related to the maximum pressure supported by the SPH elements.

**Table 6.** Reference parameters for the sensitivity analysis.

Parameters	$\gamma$	$k_0$	$A[MPa]$	$B[MPa]$	$n$	$c$	
Reference value	5.6	15,100	0.0001	695	0.35	0.05	
Variation range	<b>Min</b>	2	5000	0.0001	0.0001	0.1	0.01
	<b>Max</b>	10	30,000	10,000	10,000	1	0.2

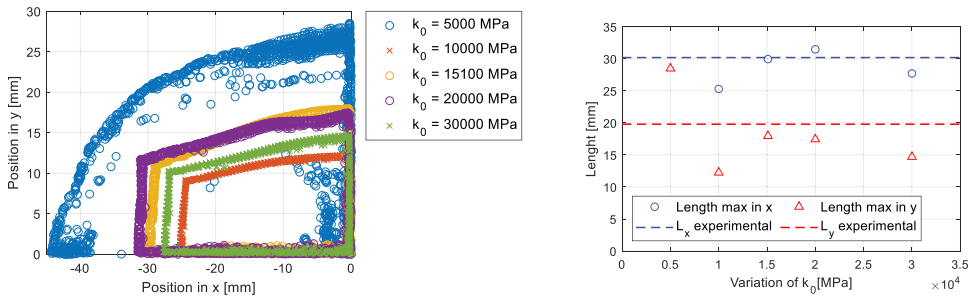


**Figure 14.** Sensitivity of the parameter  $k_0$  (contour of the final form on left and evolution of the lengths of reference on right) .<sup>[103]</sup>

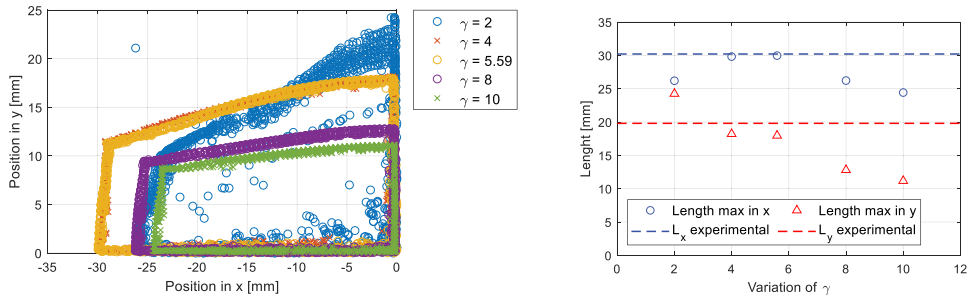


**Figure 15.** Sensitivity of the parameter Classification of fluids in rheology behaviours (contour of the final form on left and evolution of the lengths of reference on right) .<sup>[103]</sup>

### 5.3.2. Influence of plastic hardening

The A and B parameters are related to elastic-plastic behaviour, in particular to plastic hardening. The influence of the value of A parameter is shown in Figure 16. As for the  $\gamma$  parameter of the EOS, the relation between the lengths and A is not linear. But contrary to the  $\gamma$  parameter, small values of A stabilize the adhesive's extension in the longitudinal direction. Indeed, for large A values, plasticity arises later, and at the end of the simulation, elastic strains are relaxed leading to lower precision in the final geometry. For B the situation changes (see Figure 17). As B increases, the length in “y” decreases and the length in “x” increases, both slightly. This shows a lower influence of B on the final adhesive distribution. Besides that, B influences the corner shape and final form global contour.

### 5.3.3. Influence of the strain rate

The last two parameters, n (see Figure 18) and c (see Figure 19), are related to the strain rate influence. Compared with the previously-studied parameters, these two parameters show less influence. In short, the variations in the two parameters represent a linear variation for both lengths, the same behaviour as

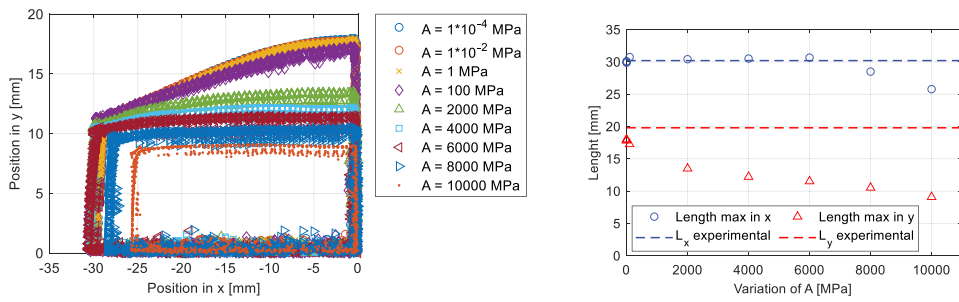


**Figure 16.** Sensitivity of the parameter  $A$  (contour of the final form on left and evolution of the lengths of reference on right) .<sup>[103]</sup>

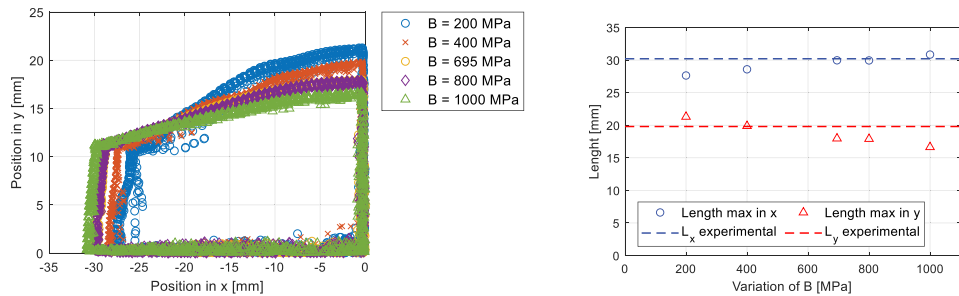


**Figure 17.** Sensitivity of the parameter  $B$  (contour of the final form on left and evolution of the lengths of reference on right) .<sup>[103]</sup>

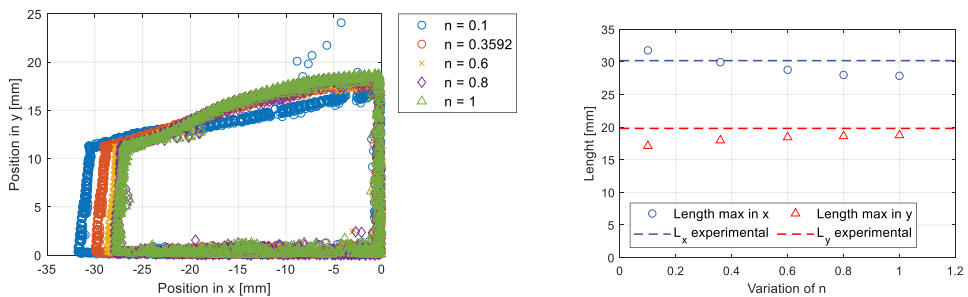


**Figure 18.** Sensitivity of the parameter  $n$  (contour of the final form on left and evolution of the lengths of reference on right) .<sup>[103]</sup>

observed for  $B$  variation but exhibiting an opposite effect. The difference is that these parameters do not change the slope of the outline curves and consequently do not change the corner format.

### 5.3.4. Self-stabilization of the squeeze process

The sensitivity analyses presented show that the SPH can be used to represent adhesive compression and final distribution, but it is important to set the parameters based on the characteristics of the adhesive. Another important

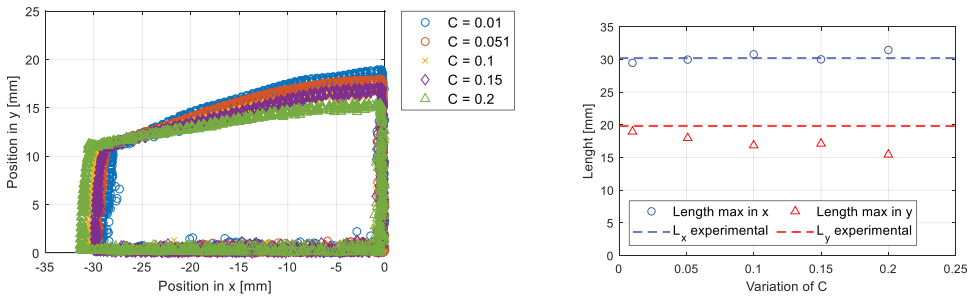


**Figure 19.** Sensitivity of the parameter  $c$  (contour of the final form on left and evolution of the lengths of reference on right) .<sup>[103]</sup>

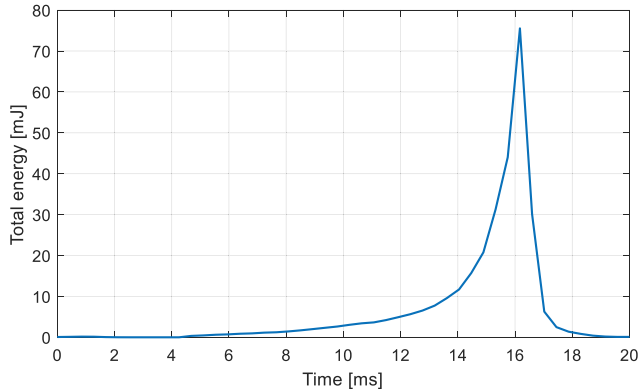


**Figure 20.** Total energy in the system during the bonding process.

aspect is the capability to naturally stop the deformation suffered by the adhesive due to the pressure applied. This phenomenon was proven to be well simulated by observing the energy evolution during the berthing process. As shown in Figure 20, after the contact between the adhesive and the moving substrate, energy begins to decrease to zero, the point at which the deformation naturally stops.

## 6. CONCLUSION

The idea of representing an adhesive using a solid behaviour law in a Lagrangian frame to simulate spreading during bonding can, at first glance, appear to be unconventional regarding the literature. This hypothesis is nevertheless a good approximation for quick and precise modelling as shown in this paper. The proposed numerical model using the Johnson-Cook behaviour law with the Murnaghan equation of state presents highly satisfactory results in predicting the final shape and covering area after stabilization of the bonding process using Lagrangian codes and SPH space discretization. The proposed

model is then an alternative solution to simulate the 3D distribution of the adhesive in the frame of generalized continuous solid mechanics. To improve the results, for instance for compressive resistance during bonding, a sensitivity analysis is necessary and could be used to optimize the mechanical properties of the adhesive based on experimental tests and for substrates of different materials or shapes (honeycomb for example). Furthermore, the model needs to be improved to predict the stress distribution during the bonding process and the residual stress or resistance force, in particular if it is intended to predict the formation of squeeze-out pudding or squeeze-out meniscus for industrial application.

## Acknowledgments

The authors thank the Ecole Doctorale MeGEP and the Université de Toulouse III - Paul Sabatier for financial support, as well as the ISAE-SUPAERO and Universidade de Porto for the provision of computational and experimental resources. In addition, the technical staff of the laboratories are warmly thanked for their contribution to this work. This work was performed in the frame of the scientific network TACCOS, meaning Toulouse Adhésion Cohésion Collage Structural (<https://personnel.isae-supaero.fr/eric-paroissien/taccos-557.html>)

## Disclosure statement

No potential conflict of interest was reported by the author(s).

## ORCID

Lorraine Aparecida Silva  <http://orcid.org/0000-0001-5420-674X>

## References

- [1] da Silva, L. F. M., D. S.; Öchsner, A.; Adams, R. D. *Handbook of Adhesion Technology*; Second; Springer. 2018; DOI: [10.1007/978-3-319-55411-2](https://doi.org/10.1007/978-3-319-55411-2).
- [2] Muravleva, L.; Squeeze Flow of Bingham, Casson and Herschel-Bulkley Fluids with Yield Slip at the Wall by Accelerated Augmented Lagrangian Method. *J Nonnewton Fluid Mech.* 2020, 282, 104320. DOI: [10.1016/j.jnnfm.2020.104320](https://doi.org/10.1016/j.jnnfm.2020.104320).
- [3] Dumont, V.; Badulescu, C.; Stamoulis, G.; Adrien, J.; Maire, E.; Lefèvre, A.; Thévenet, D. On the Influence of Mechanical Loadings on the Porosities of Structural Epoxy Adhesives Joints by Means of In-situ X-ray Microtomography. *Int. J. Adhes. Adhes.* 2020, 99, 102568. DOI: [10.1016/j.ijadhadh.2020.102568](https://doi.org/10.1016/j.ijadhadh.2020.102568).
- [4] Jaillon, A.; Étude Expérimentale Et Numérique Du Comportement À Rupture Des Assemblages Collés À Épaisseur De Couche Adhésive Variable. Doctoral dissertation. Université de Toulouse, 2020.
- [5] Banea, M. D.; da Silva, L. F. M.; RDS, C. An Overview of the Technologies for a Dhesive Debonding on Command. Ann “Dunarea Jos” Univ Galati, Fascicle XII 2013.

- [6] Bandl, C.; Kern, W.; Schlögl, S. Adhesives for “Debonding-on-demand”: Triggered Release Mechanisms and Typical Applications. *Int. J. Adhes. Adhes.* **2020**, *99*, 102585. DOI: [10.1016/j.ijadhadh.2020.102585](https://doi.org/10.1016/j.ijadhadh.2020.102585).
- [7] Bergara, T.; Castel, D.; Olive, M.; Levallois, F.; Foulc, M. Use of Debondable Structural Adhesive for Ground Testing of Gaia Segments. Proceedings of the 9th International Symposium on Materials in a Space Environment. June 16-20, 2003. Noordwijk, The Netherlands.
- [8] Meeten, G. H.; Effects of Plate Roughness in Squeeze-flow Rheometry. *J Nonnewton Fluid Mech.* **2004**, *124*(1-3), 51-60. DOI: [10.1016/j.jnnfm.2004.07.003](https://doi.org/10.1016/j.jnnfm.2004.07.003).
- [9] Jaillon, A.; Jumel, J.; Lachaud, F.; Paroissien, E.; Renart, J. Adhesive Thickness Influence on a Structural Methacrylate Adhesive Behavior. Proceedings of the 6th World Congress Adhesion and Related Phenomena (WCARP). February 25 - March 1, 2018. San Diego, United States.
- [10] Banea, M. D.; LFM, D. S.; Campilho, R. D. S. G. The Effect of Adhesive Thickness on the Mechanical Behavior of a Structural Polyurethane Adhesive. *J. Adhes.* **2014**. DOI: [10.1080/00218464.2014.903802](https://doi.org/10.1080/00218464.2014.903802).
- [11] Engmann, J.; Servais, C.; Burbidge, A. S. Squeeze Flow Theory and Applications to Rheometry: A Review. *J Nonnewton Fluid Mech.* **2005**, *132*(1-3), 1-27. DOI: [10.1016/j.jnnfm.2005.08.007](https://doi.org/10.1016/j.jnnfm.2005.08.007).
- [12] Hays, D. F.; Squeeze Films for Rectangular Plates. *J. Basic Eng.* **1963**, *85*(2), 243-246. DOI: [10.1115/1.3656568](https://doi.org/10.1115/1.3656568).
- [13] Gupta, J. L.; Vora, K. H. Analysis of Squeeze Films between Curved Annular Plates. *J. Lubr. Technol.* **1980**, *102*(1), 48-50. DOI: [10.1115/1.3251436](https://doi.org/10.1115/1.3251436).
- [14] Bujurke, N. M.; Naduvinamani, N. B.; Basti, D. P. Effect of Surface Roughness on the Squeeze Film Lubrication between Curved Annular Plates. *Ind. Lubr. Tribol.* **2007**, *59*(4), 178-185. DOI: [10.1108/00368790710753572](https://doi.org/10.1108/00368790710753572).
- [15] Chastel, T.; Mongruel, A. Squeeze Flow between a Sphere and a Textured Wall. *Phys. Fluids.* **2016**, *28*(2), 023301. DOI: [10.1063/1.4941301](https://doi.org/10.1063/1.4941301).
- [16] Préau, M.; Hubert, P. Bonded Repairs of Honeycomb Sandwich Structures: Process Monitoring and Quality Assessment. Proceedings of the 20th International Conference on Composite Materials (ICCM). July 19-24, 2015. Copenhagen, Denmark.
- [17] Yuan, C.; Li, M.; Zhang, Z.; Gu, Y. Experimental Investigation on the Co-Cure Processing of Honeycomb Structure with Self-Adhesive Prepreg. *Applied Composite Materials.* **2008**, *15*(1), 47-59. DOI: [10.1007/s10443-008-9056-4](https://doi.org/10.1007/s10443-008-9056-4).
- [18] Zienkiewicz, O. C.; Taylor, R. L. *The Finite Element Method for Fluid Dynamics*; Elsevier, Oxford, **2014**. DOI: [10.1016/C2009-0-26328-8](https://doi.org/10.1016/C2009-0-26328-8).
- [19] Kubo, M. T. K.; Rojas, M. L.; Miano, A. C.; Augusto, P. E. D. Chapter 1. *Rheological Prop Tomato Products.* **2019**, 1-25. DOI: [10.1039/9781788016247-00001](https://doi.org/10.1039/9781788016247-00001).
- [20] Ghassemi, M.; Shahidian, A. Nano and Bio Heat Transfer and Fluid Flow. Academic Press, **2017**.
- [21] Barman, P. C.; Kairi, R. R.; Das, A.; Islam, R. An Overview of Non-Newtonian Fluid. *Int. J. Appl. Sci. Eng.* **2016**, *4*(2), 97. DOI: [10.5958/2322-0465.2016.00011.3](https://doi.org/10.5958/2322-0465.2016.00011.3).
- [22] McIntyre, E. C.; Compression of Smart Materials: Squeeze Flow of Electrorheological and Magnetorheological Fluids. PhD Thesis University of Michigan, 2008.
- [23] Sherwood, J. D.; Durban, D. Squeeze Flow of a Power-law Viscoplastic Solid. *J Nonnewton Fluid Mech.* **1996**, 1395-1400. DOI: [10.1016/0377-0257\(95](https://doi.org/10.1016/0377-0257(95).
- [24] Fusi, L.; Farina, A.; Rosso, F. On the No-slip Boundary Conditions for Squeeze Flow of Viscous Fluids. *Mech. Res. Commun.* **2015**, *70*, 1-3. DOI: [10.1016/j.jnnfm.2005.08.007](https://doi.org/10.1016/j.jnnfm.2005.08.007).

- [25] Laun, H. M.; Rady, M.; Hassager, O. Analytical Solutions for Squeeze Flow with Partial Wall Slip. *J Nonnewton Fluid Mech.* 1999, 81(1–2), 1–15. DOI: [10.1016/j.jnnfm.2005.08.007](https://doi.org/10.1016/j.jnnfm.2005.08.007).
- [26] Meeten, G. H.; Constant-force Squeeze Flow of Soft Solids. *Rheol. Acta.* 2002, 41(6), 557–566. DOI: [10.1007/s00397-002-0241-3](https://doi.org/10.1007/s00397-002-0241-3).
- [27] Shaikat, A.; Sharma, A.; Joshi, Y. M. Squeeze Flow Behavior of (Soft Glassy) Thixotropic Material. *J Nonnewton Fluid Mech* 2012, 167–168, 9–17. DOI: [10.1016/j.jnnfm.2011.09.006](https://doi.org/10.1016/j.jnnfm.2011.09.006).
- [28] Uzal, A.; Spangenberg, J.; Nielsen, M. W.; Sonne, M. R.; Hattel, J. H. Numerical Modelling of the Bonding Process for Wind Turbine Blades: Model Validation. Proceedings of the 21st International Conference on Composite Materials (ICCM-21). August 20–25, 2017. Xi'an, China.
- [29] Fusi, L.; Farina, A.; Rosso, F. Planar Squeeze Flow of a Bingham Fluid. *J Nonnewton Fluid Mech.* 2015, 225, 1–9. DOI: [10.1016/j.jnnfm.2015.08.004](https://doi.org/10.1016/j.jnnfm.2015.08.004).
- [30] Yang, S. P.; Zhu, K. Q. Analytical Solutions for Squeeze Flow of Bingham Fluid with Navier Slip Condition. *J Nonnewton Fluid Mech.* 2006, 138(2–3), 173–180. DOI: [10.1016/j.jnnfm.2006.05.007](https://doi.org/10.1016/j.jnnfm.2006.05.007).
- [31] Park, J. M.; Flow Classification of Radial and Squeeze Flows between Parallel Disks. *J Nonnewton Fluid Mech.* 2020, 286, 104416. DOI: [10.1108/00368790710753572](https://doi.org/10.1108/00368790710753572).
- [32] Adams, M. J.; Edmondson, B.; Caughey, D. G.; Yahya, R. An Experimental and Theoretical Study of the Squeeze-film Deformation and Flow of Elastoplastic Fluids. *J Nonnewton Fluid Mech.* 1994, 51(1), 61–78. DOI: [10.1016/0377-0257\(94\)85003-8](https://doi.org/10.1016/0377-0257(94)85003-8).
- [33] Muravleva, L.; Squeeze Flow of Bingham, Casson and Herschel-Bulkley Fluids with Yield Slip at the Wall by Accelerated Augmented Lagrangian Method. *J Nonnewton Fluid Mech.* 2020, 282, 104320. DOI: [10.1016/j.jnnfm.2020.104320](https://doi.org/10.1016/j.jnnfm.2020.104320).
- [34] Bergamasco, L.; Izquierdo, S.; Duvivier, E.; Royo, J. M.; Chiminelli, A.; Jiménez, M. A. Generalized Analytical Solution for Compressive Forces in Adhesively-bonded-joint Assembling. *Int. J. Adhes. Adhes.* 2014, 52, 26–30. DOI: [10.1016/j.ijadhadh.2014.03.010](https://doi.org/10.1016/j.ijadhadh.2014.03.010).
- [35] Sherwood, J. D.; Durban, D. Squeeze-flow of a Herschel–Bulkley Fluid. *J Nonnewton Fluid Mech.* 1998, 77(1–2), 115–121. DOI: [10.1016/S0377-0257\(97\)00099-2](https://doi.org/10.1016/S0377-0257(97)00099-2).
- [36] Liu, L.; Cai, M.; Luo, G.; Zhao, Z.; Chen, W. Macroscopic Numerical Simulation Method of Multi-phase STF-impregnated Kevlar Fabrics. Part 2: Material Model and Numerical Simulation. *Composite Structures.* 2021, 262, 113662. DOI: [10.1016/j.compstruct.2021.113662](https://doi.org/10.1016/j.compstruct.2021.113662).
- [37] Singh, U. P.; Gupta, R. S. Non-Newtonian Effects on the Squeeze Film Characteristics between a Sphere and a Flat Plate: Rabinowitsch Model. *Adv. Tribol.* 2012, 2012, 1–7. DOI: [10.1155/2012/571036](https://doi.org/10.1155/2012/571036).
- [38] Singh, U. P.; Gupta, R. S.; Kapur, V. K. On the Squeeze Film Characteristics between a Long Cylinder and a Flat Plate: Rabinowitsch Model. *Proc. Inst. Mech. Eng. Part J J. Eng. Tribol.* 2013, 227(1), 34–42. DOI: [10.1063/1.4941301](https://doi.org/10.1063/1.4941301).
- [39] Phan-thien, N.; Sugeng, F.; Tanner, R. I. The Squeeze-film Flow of a Viscoelastic Fluid. *J Nonnewton Fluid Mech.* 1987, 24(1), 97–119. DOI: [10.1016/0377-0257\(87\)85006-1](https://doi.org/10.1016/0377-0257(87)85006-1).
- [40] Delhaye, N.; Poitou, A.; Chaouche, M. Squeeze Flow of Highly Concentrated Suspensions of Spheres. *J Nonnewton Fluid Mech.* 2000, 94(1), 67–74. DOI: [10.1016/S0377-0257\(00\)00130-0](https://doi.org/10.1016/S0377-0257(00)00130-0).
- [41] Sapinski, B.; Horak, W.; Sioma, A. Experiments of MR Fluid Behaviour in the Squeeze Mode Using the Vision Method. Proceedings of the 15th International Carpathian Control Conference. May 28–30, 2014. Velke Karlovice, Czech Republic. doi:[10.1109/CarpathianCC.2014.6843658](https://doi.org/10.1109/CarpathianCC.2014.6843658).

- [42] Bin Mazlan, S. A.; The Behaviour of Magnetorheological Fluids in Squeeze Mode. Doctoral dissertation. Dublin City University, 2008.
- [43] Lett, C.; Verley, P.; Mullon, C.; Parada, C.; Brochier, T.; Penven, P.; Blanke, B. A Lagrangian Tool for Modelling Ichthyoplankton Dynamics. *Environ Model Softw.* 2008, 23(9), 1210–1214. DOI: [10.1016/j.envsoft.2008.02.005](https://doi.org/10.1016/j.envsoft.2008.02.005).
- [44] Rossi, V.; Ser-Giacomi, E.; Dubois, M.; Monroy, P.; Hidalgo, M.; Hernández-García, E.; López, C. Lagrangian Flow Networks: A New Framework to Study the Multi-scale Connectivity and the Structural Complexity of Marine Populations. Proceedings of the CIESM International Research Workshop, Monaco. 2016.
- [45] Spangenberg, J.; Roussel, N.; Hattel, J. H.; Stang, H.; Skocek, J.; Geiker, M. R. Flow Induced Particle Migration in Fresh Concrete: Theoretical Frame, Numerical Simulations and Experimental Results on Model Fluids. *Cem. Concr. Res.* 2012, 42(4), 633–641. DOI: [10.1016/j.cemconres.2012.01.007](https://doi.org/10.1016/j.cemconres.2012.01.007).
- [46] Roussel, N.; Gram, A.; Cremonesi, M.; Ferrara, L.; Krenzer, K.; Mechtcherine, V.; Shyshko, S.; Skocek, J.; Spangenberg, J.; Svec, O., et al. Numerical Simulations of Concrete Flow: A Benchmark Comparison. *Cem. Concr. Res.* 2016, 79, 265–271. DOI: [10.1016/j.cemconres.2015.09.022](https://doi.org/10.1016/j.cemconres.2015.09.022).
- [47] Costa, E. B. C.; de França, M. S.; Bergossi, F. L. N.; Borges, R. K. Squeeze Flow of Mortars on Brick Substrate and Its Relation with Bond Strength. *Constr. Build. Mater.* 2020, 265, 120298. DOI: [10.1016/j.conbuildmat.2020.120298](https://doi.org/10.1016/j.conbuildmat.2020.120298).
- [48] Bernabeu, N.; Modélisation Multi-physique Des Écoulements Viscoplastiques: Application Aux Coulées De Lave Volcanique. PhD Thesis Université Grenoble Alpes (ComUE), 2015.
- [49] Garel, F.; Kaminski, E.; Tait, S.; Limare, A. An Analogue Study of the Influence of Solidification on the Advance and Surface Thermal Signature of Lava Flows. *Earth Planet. Sci. Lett.* 2014, 396, 46–55. DOI: [10.1016/j.epsl.2014.03.061](https://doi.org/10.1016/j.epsl.2014.03.061).
- [50] Hamrock, B.J.; Schmid, S. R.; Jacobson, B. O. Fundamentals of Fluid Film Lubrication. Marcel Dekker; 2004.
- [51] Patel, M. J.; Blackburn, S.; Wilson, D. I. Modelling of Pastes as Viscous Soils – Lubricated Squeeze Flow. *Powder Technol.* 2018, 323, 250–268. DOI: [10.1016/j.powtec.2017.09.052](https://doi.org/10.1016/j.powtec.2017.09.052).
- [52] Campanella, O. H.; Peleg, M. Squeezing Flow Viscometry for Nonelastic Semiliquid Foods — Theory and Applications. *Crit. Rev. Food Sci. Nutr.* 2002, 42(3), 241–264. DOI: [10.1080/10408690290825547](https://doi.org/10.1080/10408690290825547).
- [53] Campanella, O. H.; Peleg, M. Squeezing Flow Viscosimetry of Peanut Butter. *J. Food Sci.* 1987, 52(1), 180–184. DOI: [10.1111/j.1365-2621.1987.tb14000.x](https://doi.org/10.1111/j.1365-2621.1987.tb14000.x).
- [54] Spangenberg, J.; Uzal, A.; Nielsen, M. W.; Hattel, J. H. A Robustness Analysis of the Bonding Process of Joints in Wind Turbine Blades. *Int. J. Adhes. Adhes.* 2018, 85, 281–285. DOI: [10.1016/j.ijadhadh.2018.06.009](https://doi.org/10.1016/j.ijadhadh.2018.06.009).
- [55] Han, W.; Berthet, F.; Dusserre, G.; Schmidt, F. Modelling the Shape of an Adhesive Joint during Assembly. Proceedings of the 8th International Conference on Structural Analysis of Advanced Materials (ICSAAM 2018). August 28-31, 2018. Tarbes, France.
- [56] Liu, M. B.; Liu, G. R. Smoothed Particle Hydrodynamics (SPH): An Overview and Recent Developments. *Arch. Comput. Methods Eng.* 2010. DOI: [10.1007/s11831-010-9040-7](https://doi.org/10.1007/s11831-010-9040-7).
- [57] Breinlinger, T.; Polfer, P.; Hashibon, A.; Kraft, T. Surface Tension and Wetting Effects with Smoothed Particle Hydrodynamics. *J. Comput. Phys.* 2013, 243, 14–27. DOI: [10.1016/j.jcp.2013.02.038](https://doi.org/10.1016/j.jcp.2013.02.038).
- [58] Anderson, J. D. Computational Fluid Dynamics: The Basics with Applications. McGraw-Hill, 1995



- [59] Paiva, A.; Uma Abordagem Lagrangeana Para Simulação De Escoamentos De Fluidos Viscoplasticos E Multifasicos. Tese de Doutorado, Pontificia Universidade Católica do Rio de Janeiro, 2007.
- [60] Ferziger, J. H.; Perić, M. Computational Methods for Fluid Dynamics. Springer, Berlin. 2012. DOI: 10.1007/978-3-642-97651-3.
- [61] Sarrate, J.; Huerta, A.; Donea, J. Arbitrary Lagrangian–Eulerian Formulation for Fluid–rigid Body Interaction. *Comput. Methods Appl. Mech. Eng.* 2001, 190(24–25), 3171–3188. DOI: 10.1016/S0045-7825(00)00387-X.
- [62] Rapp, B. E.; *Microfluidics: Modelling, Mechanics and Mathematics*; Elsevier, Oxford, 2017. DOI: 10.1016/C2012-0-02230-2.
- [63] Müller, M.; Finke, J.; Stahl, L.; Tong, Y.; Fricke, H.; Vallée, T. Development and Validation of a Compression Flow Model of non-Newtonian Adhesives. *J. Adhes.* 2021, 1–38. DOI: 10.1080/00218464.2021.1895771.
- [64] Eymard, R.; Gallouët, T.; Herbin, R. Finite Volume Methods. *Handb Numer Anal.* 2000. DOI: 10.1016/S1570-8659(00)07005-8.
- [65] Il, K. Y.; Lim, E.; Song, Y. S. Simulation of Injection-compression Molding for Thin and Large Battery Housing. *Curr. Appl. Phys.* 2018. DOI: 10.1016/j.cap.2018.08.017.
- [66] Evans, A. D.; Qian, C. C.; Turner, T. A.; Harper, L. T.; Warrior, N. A. Flow Characteristics of Carbon Fibre Moulding Compounds. *Compos. Part A Appl. Sci. Manuf.* 2016, 90, 1–12. DOI: 10.1016/j.compositesa.2016.06.020.
- [67] Chen, Z.; Huang, T.; Shao, Y.; Li, Y.; Xu, H.; Avery, K.; Zeng, D.; Chen, W.; Su, X. Multiscale Finite Element Modeling of Sheet Molding Compound (SMC) Composite Structure Based on Stochastic Mesostructure Reconstruction. *Compos. Struct.* 2018. DOI: 10.1016/j.compstruct.2017.12.039.
- [68] Burka, P.; Liu, X.; Thompson, M. C.; Sheridan, J. Modelling of Adhesive Bonding for Aircraft Structures Applying the Insertion Squeeze Flow Method. *Compos. Part B Eng.* 2013, 50, 247–252. DOI: 10.1016/j.compositesb.2013.02.019.
- [69] Baker, A. J.; Finite Element Analysis in Computational Fluid Mechanics. *Nucl. Simul.* 1987. DOI: 10.1007/978-3-642-83221-5\_7.
- [70] Finite Element, G. R.; Methods For Navier-Stokes Equations. *Annu. Rev. Fluid Mech.* 1992. DOI: 10.1146/annurev.fluid.24.1.167.
- [71] Pironneau, O. *Finite Element Methods for Fluids*; Wiley Chichester, Ivry sur Seine. 1992; Vol. 72. .
- [72] Takashi, N.; Hughes, T. J. R. An Arbitrary Lagrangian-Eulerian Finite Element Method for Interaction of Fluid and a Rigid Body. *Comput. Methods Appl. Mech. Eng.* 1992, 95 (1), 115–138. DOI: 10.1016/0045-7825(92)90085-X.
- [73] Tezduyar, T. E.; Behr, M.; Liou, J. A New Strategy for Finite Element Computations Involving Moving Boundaries and interfaces-The Deforming-spatial-domain/space-time Procedure: I. The Concept and the Preliminary Numerical Tests. *Comput. Methods Appl. Mech. Eng.* 1992. DOI: 10.1016/0045-7825(92)90059-S.
- [74] Johnson, A. A.; Tezduyar, T. E. Mesh Update Strategies in Parallel Finite Element Computations of Flow Problems with Moving Boundaries and Interfaces. *Comput. Methods Appl. Mech. Eng.* 1994, 119(1–2), 73–94. DOI: 10.1016/0045-7825(94)00077-8.
- [75] Rannacher, R. Finite Element Methods for the Incompressible Navier-Stokes Equations. *Fundam. Dir. Math. Fluid Mech.* 2011. DOI: 10.1007/978-3-0348-8424-2\_6.
- [76] Hughes, T. J. R.; Liu, W. K.; Brooks, A. Finite Element Analysis of Incompressible Viscous Flows by the Penalty Function Formulation. *J. Comput. Phys.* 1979, 30(1), 1–60. DOI: 10.1016/0021-9991(79)90086-X.
- [77] Oden, J. T.; Wellford, L. C. Analysis of Flow of Viscous Fluids by the Finite-element Method. *AIAA J.* 1972, 10(12), 1590–1599. DOI: 10.2514/3.6691.

- [78] Adams, M. J.; Aydin, I.; Briscoe, B. J.; Sinha, S. K. A Finite Element Analysis of the Squeeze Flow of an Elasto-viscoplastic Paste Material. *J Nonnewton Fluid Mech.* 1997, 71 (1–2), 41–57. DOI: [10.1016/S0377-0257\(96\)01546-7](https://doi.org/10.1016/S0377-0257(96)01546-7).
- [79] Abali, B. E. An Accurate Finite Element Method for the Numerical Solution of Isothermal and Incompressible Flow of Viscous Fluid. *Fluids.* 2019, 4(1), 5. DOI: [10.3390/fluids4010005](https://doi.org/10.3390/fluids4010005).
- [80] Rizzo, F.; Pinto, F.; Meo, M. Investigation of Silica-Based Shear Thickening Fluid in Enhancing Composite Impact Resistance. *Appl. Compos. Mater.* 2020, 27(3), 209–229. DOI: [10.1007/S10443-020-09805-7](https://doi.org/10.1007/S10443-020-09805-7).
- [81] Gürgen, S. Numerical Modeling of Fabrics Treated with Multi-phase Shear Thickening Fluids under High Velocity Impacts. *Thin-Walled Struct.* 2020, 148, 106573. DOI: [10.1016/J.TWS.2019.106573](https://doi.org/10.1016/J.TWS.2019.106573).
- [82] Liu, G. R.; Liu, M. B. Smoothed Particle Hydrodynamics - A Meshfree Particle Method. World Scientific Publishing Co Pte Ltd ,2010. DOI: [10.1142/9789812564405](https://doi.org/10.1142/9789812564405).
- [83] Gingold, R. A.; Monaghan, J. J. Smoothed Particle Hydrodynamics: Theory and Application to Non-spherical Stars. *Mon Not R Astron Soc.* 1977, 181(3), 375–389. DOI: [10.1093/mnras/181.3.375](https://doi.org/10.1093/mnras/181.3.375).
- [84] Lucy, L. B. A Numerical Approach to the Testing of the Fission Hypothesis. *Astron J.* 1977, 82, 1013. DOI: [10.1086/112164](https://doi.org/10.1086/112164).
- [85] Gingold, R.; Monaghan, J. Kernel Estimates as a Basis for General Particle Methods in Hydrodynamics. *J. Comput. Phys.* 1982, 46(3), 429–453. DOI: [10.1016/0021-9991\(82\)90025-0](https://doi.org/10.1016/0021-9991(82)90025-0).
- [86] Randles, P. W.; Libersky, L. D. Smoothed Particle Hydrodynamics: Some Recent Improvements and Applications. *Comput. Methods Appl. Mech. Eng.* 1996, 139(1–4), 375–408. DOI: [10.1016/S0045-7825\(96\)01090-0](https://doi.org/10.1016/S0045-7825(96)01090-0).
- [87] Monaghan, J. J.. Smoothed Particle Hydrodynamics. *Annu Rev Astron Astrophys.* 1992, 30(1), 543–574. DOI: [10.1146/annurev.aa.30.090192.002551](https://doi.org/10.1146/annurev.aa.30.090192.002551).
- [88] Weaver, T.; Xiao, Z. Fluid Simulation by the Smoothed Particle Hydrodynamics Method: A Survey. Proceedings of the VISIGRAPP, 27-29 February, 2016. Rome, Italy. DOI: [10.5220/0005673702130223](https://doi.org/10.5220/0005673702130223).
- [89] Pelfrene, J. Study of the SPH Method for Simulation of Regular and Breaking Waves. *Master Thesis Universiteit Gent*, 2011.
- [90] Oger, G.; Aspects Théoriques De La Méthode SPH Et Applications À L'hydrodynamique À Surface Libre. PhD Thesis École Centrale de Nantes, 2006.
- [91] Monaghan, J. J. Simulating Free Surface Flows with SPH. *J. Comput. Phys.* 1994, 110(2), 399–406. DOI: [10.1006/jcph.1994.1034](https://doi.org/10.1006/jcph.1994.1034).
- [92] Cherfil, J.-M.; Développements Et Applications De La Méthode SPH Aux Écoulements Visqueux À Surface Libre. Mécanique [physics.med-ph]. Université du Havre, 2011.
- [93] Morris, J. P.; Fox, P. J.; Zhu, Y. Modeling Low Reynolds Number Incompressible Flows Using SPH. *J. Comput. Phys.* 1997, 136(1), 214–226. DOI: [10.1006/jcph.1997.5776](https://doi.org/10.1006/jcph.1997.5776).
- [94] Zisis, I.; Messahel, R.; Boudlal, A.; Van Der Linden, B.; Koren, B. Validation of Robust SPH Schemes for Fully Compressible Multiphase Flows. *Int J Multiphys.* 2015, 9(3), 225–234. DOI: [10.1260/1750-9548.9.3.225](https://doi.org/10.1260/1750-9548.9.3.225).
- [95] Colagrossi, A.; Landrini, M. Numerical Simulation of Interfacial Flows by Smoothed Particle Hydrodynamics. *J. Comput. Phys.* 2003, 191(2), 448–475. DOI: [10.1016/S0021-9991\(03\)00324-3](https://doi.org/10.1016/S0021-9991(03)00324-3).
- [96] Monaghan, J. J.; Kocharyan, A. SPH Simulation of Multi-phase Flow. *Comput. Phys. Commun.* 1995, 87(1–2), 225–235. DOI: [10.1016/0010-4655\(94\)00174-Z](https://doi.org/10.1016/0010-4655(94)00174-Z).
- [97] Antoci, C.; Gallati, M.; Sibilla, S. Numerical Simulation of Fluid–structure Interaction by SPH. *Comput. Struct.* 2007, 85(11–14), 879–890. DOI: [10.1016/j.compstruc.2007.01.002](https://doi.org/10.1016/j.compstruc.2007.01.002).

- [98] Queiroz, T. E. Animação Computacional De Escoamento De Fluidos Utilizando O Método SPH. PhD Thesis Universidade de São Paulo, 2008. doi:10.11606/D.55.2008.tde-10112008-110933.
- [99] Schechter, H. Enhancing Particle Methods for Fluid Simulation in Computer Graphics. Doctoral dissertation, University of British Columbia, 2013.
- [100] Ansanay-Alex, G. Un Schéma Éléments Finis Non-conformes/volumes Finis Pour L'approximation En Maillages Non-structures Des Écoulements a Faible Nombre De Mach. Doctoral dissertation. Université de Provence, 2009.
- [101] Quenjel, E. H. Volumes finis/Éléments Finis Pour Des Écoulements Diphasiques Compressibles En Milieux Poreux Hétérogènes Et Anisotropes. Doctoral dissertation. Ecole Centrale de Nantes et Université Moulay Ismail Meknes, 2018.
- [102] Livermore Software Technology Corporation (LSTC). LS-DYNA® Keyword User's Manual – Volume II – Material Models – R9.0. 2016.
- [103] Silva, L. A.; Espinosa, C.; LFM, D. S.; Paroissien, E.; Lachaud, F. Simulation of Adhesive Squeeze Flow Using Smoothed Particle Hydrodynamics. Proceedings of the *Conference Comput. Methods Multi-scale, Multi-uncertainty Multi-physics Problems*. July 19-22, 2019. Porto, Portugal.